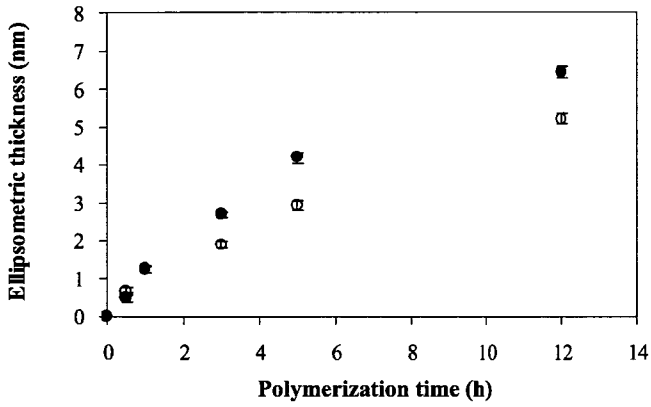

Fig. 1. Ellipsometric thickness of polymer brushes versus polymerization time for targeted DP = 200: (●) PMPC and (○) P*t*-BMA.

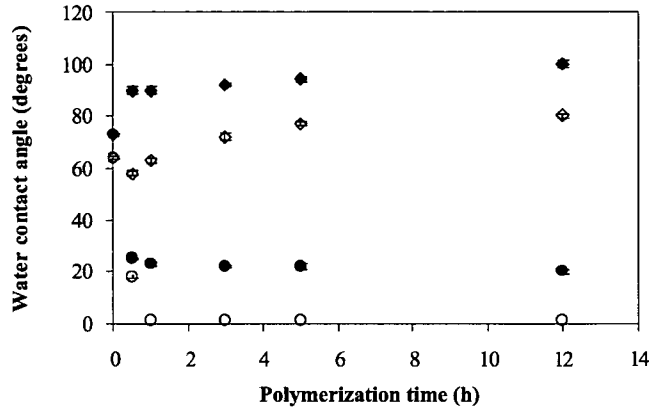

Fig. 2. Water contact angle data of polymer brushes versus polymerization time for PMPC: (●) θ_A, (○) θ_R and P*t*-BMA: (◆) θ_A, (◇) θ_R.

micropatterned surface-tethered PMPC brushes to manipulate proteins and cells. Evidently, the bovine serum albumin and fibroblast cells selectively adhered on the areas where there was an absence of PMPC brushes having a thickness greater than 5.5 ± 1.0 nm.

Later, Feng and co-workers have investigated the adsorption of proteins on the PMPC brushes. They have found that the suppression of protein adsorption from protein mixtures (fibrinogen and lysozyme) was not strongly dependent on protein size and charge [37]. Also, the effect of the graft density of the PMPC brushes on the adsorption of fibrinogen was more profound than that of the chain length [38]. To control the graft density of PMPC brushes, they have used silicon substrates having a mixed composition of α-bromoester groups (initiating sites) and alkyl groups (diluting groups) through a competitive chemisorption of 10-(2-bromo-2-methyl)propionyloxydecyltrichlorosilane and decyltrichlorosilane on the silicon substrates. Here we use an alternative approach, a two-step process involving a subsequent reaction of the partially modified surface by tris(TMS) with the silane carrying initiating sites, 3-(2-bromoisobutyryl)propyl dimethylethoxysilane. Intuitively, the individual reactions using single components should be more controllable and reproducible, yielding more ordered and better packed monolayers, than the competitive chemisorption using mixed silanes [39]. The control of the nanoscopic spatial distribution of the surface-tethered polymer brushes should also be effective.

To test the ability to control the growth of polymer brushes, the SIP was first conducted on the silicon-supported α-bromoisobutyrate monolayer. As measured by ellipsometry, the thickness of the α-bromoisobutyrate monolayers was 9.3 ± 0.1 Å. Fig. 1 shows the development of PMPC and P*t*-BMA thickness as a function of time at a targeted degree of polymerization (DP) of 200. Obviously, the thickness increased with time, suggesting that polymerization time can be used as a tool for controlling the growth of polymer brushes. The formation of polymer brushes was also verified by contact angle analysis. According to Fig. 2, both advancing (θ_A) and receding (θ_R) water contact angles of the silicon-supported α-bromoisobutyrate monolayer drastically changed from 72°/68° to ~20°/1° for the hydrophilic silicon-supported PMPC brushes and to ~100°/80° for the hydrophobic silicon-supported P*t*-BMA brushes

Previous work reported by Ejaz and co-workers [40] has demonstrated that the molecular weight of "free" polymer formed in the solution from the "sacrificial" or "added" initiator closely resembled that of the grafted polymer brushes cleaved from the surface. Thus, it can be used to monitor the SIP process. The fact that the molecular weight increases linearly with polymerization time and the molecular weight distribution is close to 1.0 for both PMPC and P*t*-BMA (data not shown) suggested that the polymerization was well controlled and the mechanism is living. The molecular weight ($\overline{M}_n$) of free polymer together with the ellipsometric thickness (t) of the grafted polymer brushes can be used to estimate the graft density (σ), which is the inverse of cross-sectional area (A_x) per chain of polymer brushes:

$$\sigma = \frac{1}{A_x} = \frac{t\rho N_A}{M}, \tag{3}$$

where ρ is the mass density (1.30 g/cm^3 for PMPC and 1.10 g/cm^3 for P*t*-BMA) and N_A is the Avogadro number. Using slopes obtained from the plots in Fig. 3, which correspond to t/M, the calculated graft densities of PMPC and P*t*-BMA brushes for the targeted DP = 200 are 0.46 and 0.25 chains/nm^2, respectively. Although dimethylethoxysilane was used for the preparation of the surface-tethered initiator, the graft density of the polymer brushes obtained from our studies are in the same range as the graft density of the polymer brushes prepared by surface-initiated ATRP using trichlorosilane for the preparation of the surface-tethered initiator (0.1 to 0.6 chains/nm^2) [11,13,35].

This part of the investigation has demonstrated that the formation of both PMPC and P*t*-BMA brushes by SIP from the surface bearing a α-bromoisobutyrate monolayer via the ATRP mechanism can be well controlled in terms of thickness, molecular weight, and molecular weight distribution, and the polymerization process is living.

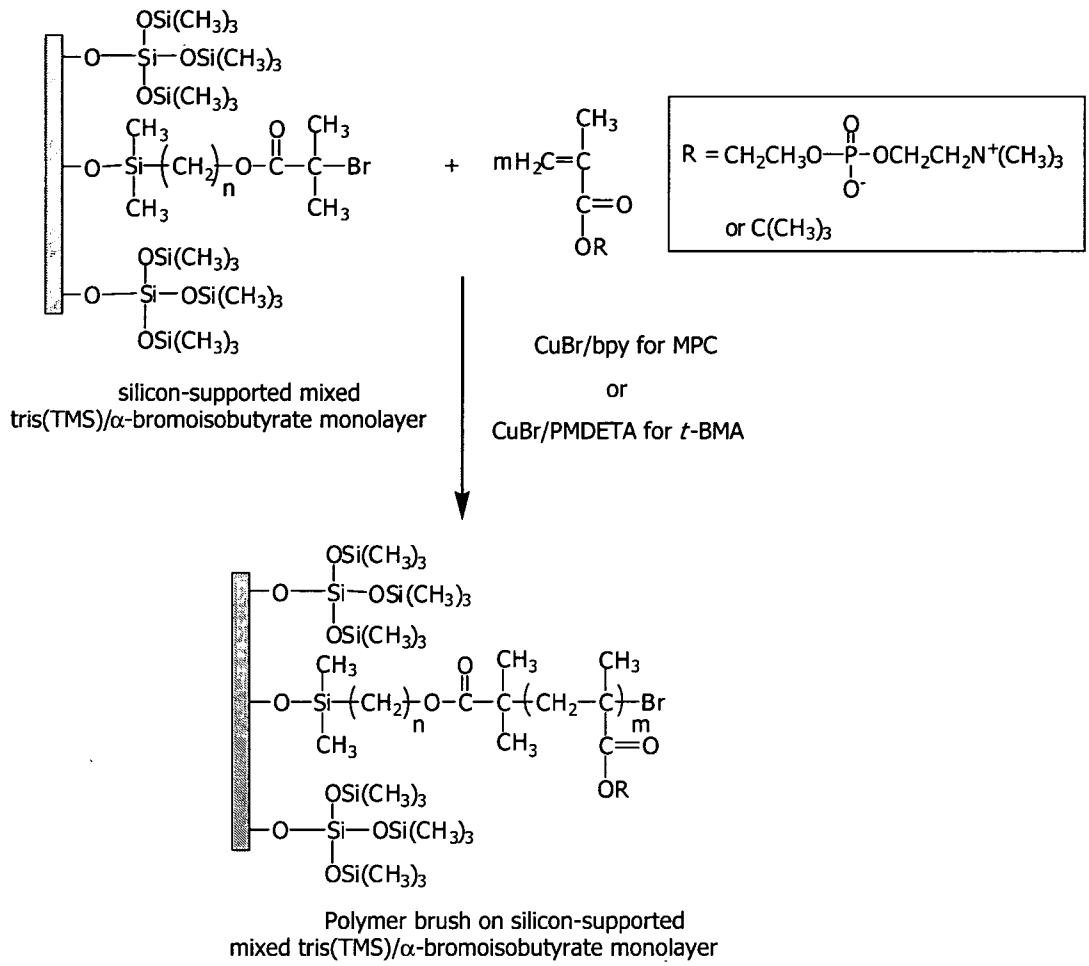

Scheme 2. Surface-initiated polymerization on silicon-supported mixed tris(TMS)/α-bromoisobutyrate monolayer.

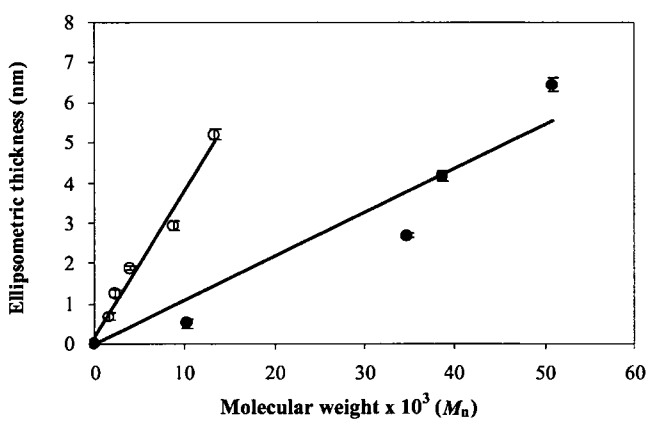

Fig. 3. Relationship between the ellipsometric thickness of polymer brushes and the molecular weight ($\bar{M}_n$) of free (●) PMPC and (○) P*t*-BMA.

3.3. *Surface-initiated polymerization on silicon-supported mixed tris(TMS)/α-bromoisobutyrate monolayers*

The silicon-supported mixed tris(TMS)/α-bromoisobutyrate monolayers was intended to be used as a nanoscale template for the formation of polymer brushes (Scheme 2). The growth of polymer brushes as a function of %tris(TMS) coverage and polymerization time is primarily discussed in terms of water contact angle and ellipsometric thickness. Using 5 h of polymerization, the thickness of PMPC and P*t*-BMA brushes, which is related to the density and length of polymer brushes, decreased as the %tris(TMS) coverage increased (Fig. 4). In contrast, the advancing and receding water contact angles of the mixed tris(TMS)/PMPC brushes shown in Fig. 5 proportionally increase with %tris(TMS) coverage. As a consequence of comparable hydrophobicity between the tris(TMS) monolayer ($\theta_A/\theta_R = 92°/82°$) and P*t*-BMA ($\theta_A/\theta_R = 100°/80°$), the water contact angle of the grafted P*t*-BMA brushes grown from the tris(TMS)/α-bromoisobutyrate monolayer was almost independent of %tris(TMS) coverage. It should be noted that the growth of polymer brushes from nanopores can also be tuned by the polymerization time (data not shown).

Originally, the observation that a surface having a certain %tris(TMS) coverage (~15–20 Å) is relatively thicker than an α-bromoisobutyrate monolayer (~10 Å) brought a concern that the short alkyl spacer between the surface-immobilized end and the other end bearing the α-bromoisobutyrate group, especially for $n = 3$, might be buried in the nanopores surrounded by tris(TMS) and unable to initiate polymerization. Although

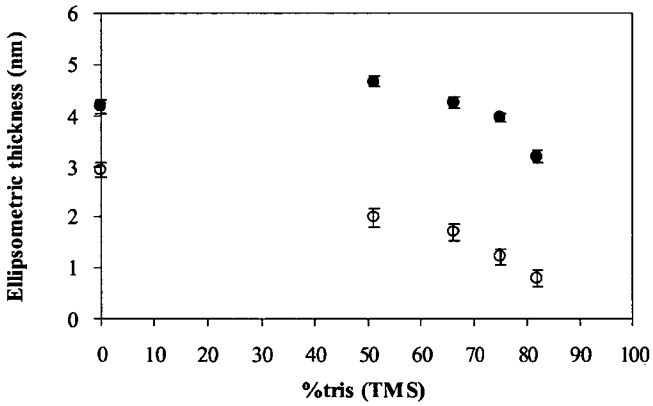

Fig. 4. Ellipsometric thickness of (●) PMPC and (○) P*t*-BMA brushes grown from the silicon-supported mixed tris(TMS)/α-bromoisobutyrate monolayer using a polymerization time of 5 h as a function of tris(TMS) coverage.

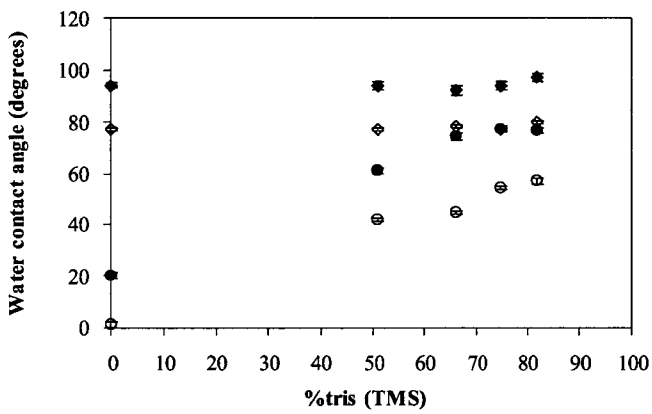

Fig. 5. Water contact angle of polymer brushes grown from the silicon-supported mixed tris(TMS)/α-bromoisobutyrate monolayer using a polymerization time of 5 h as a function of tris(TMS) coverage: PMPC: (●) θ_A, (○) θ_R and P*t*-BMA: (◆) θ_A, (◇) θ_R.

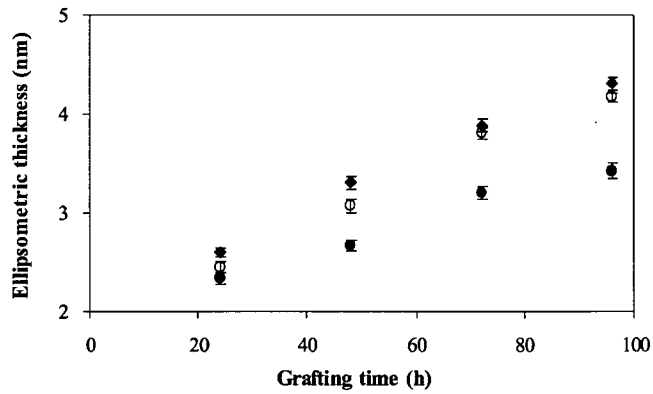

Fig. 6. Ellipsometric thickness of PMPC brushes grown from silicon-supported mixed 82% tris(TMS)/α-bromoisobutyrate monolayers versus grafting time of initiator using polymerization time of 5 h: (●) n_3, (○) n_6, and (◆) n_{10}.

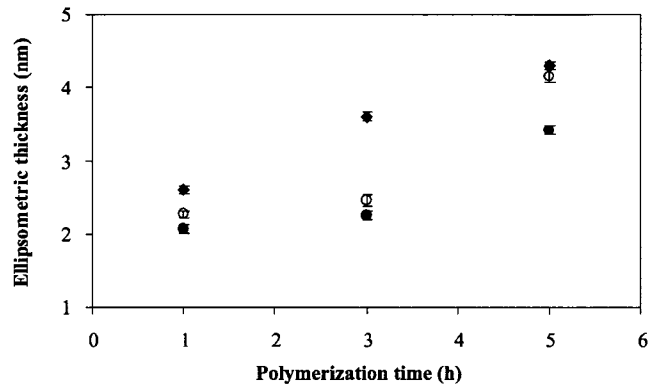

Fig. 7. Ellipsometric thickness of PMPC brushes grown from silicon-supported mixed 82% tris(TMS)/α-bromoisobutyrate monolayers versus polymerization time using grafting time of initiator of 96 h: (●) n_3, (○) n_6, and (◆) n_{10}.

the evidence shown above suggested otherwise, we still attempted to use two more analogous series of end-functionalized α-bromoisobutyrate silane compounds having longer spacers ($n = 6$ and 10) to react with the residual silanols in nanopores in order to determine the effect of the alkyl spacer on the efficiency of SIP. The immobilized α-bromoisobutyrate initiator is defined according to its alkyl spacer, denoting propyl ($n = 3$), hexyl ($n = 6$) and decyl ($n = 10$) as n_3, n_6, and n_{10}, respectively. The ellipsometric thicknesses of the silicon-supported α-bromoisobutyrate monolayers of n_6 and n_{10} are 15 and 18 Å, respectively.

Fig. 6 depicts the thickness of PMPC brushes grown from the silicon-supported mixed tris(TMS)/α-bromoisobutyrate monolayer having 82% tris(TMS) coverage. The density of the surface-tethered initiator was varied as function of grafting time in the range of 24–96 h. Polymerization was then carried out for 5 h. For a similar graft density of initiator (using the same grafting time), the thicknesses of PMPC brushes grown from n_6 and n_{10} are higher than those of PMPC brushes grown from n_3. This outcome can possibly be explained by the better mobility and the longer alkyl spacer of n_6 and n_{10}, allowing them to overcome the steric hindrance of the surrounding tris(TMS) and to reach monomers more efficiently than n_3. It can also be observed that the higher the graft density or the longer the grafting time of initiator, the denser and the thicker the PMPC brushes.

Using the grafting time of 96 h for all three initiators, the kinetics of surface-initiated polymerization of MPC on silicon-supported mixed tris(TMS)/α-bromoisobutyrate monolayers (n_3, n_6, and n_{10}) having 82% tris(TMS) coverage were determined. The thickness of PMPC brushes as a function of polymerization time is illustrated in Fig. 7. These data clearly suggest that not only does the alkyl spacer influence the ability of α-bromoisobutyrate to react with the monomers but also how fast it can react. The data points at 3 h can distinguish between the kinetics of n_6 and n_{10} at an early stage of polymerization. Nonetheless, such dissimilarity is no longer noticeable after a longer polymerization time.

3.4. Surface topography of polymer brushes in nanopores

AFM was used as a tool to monitor the surface topography of the grafted polymer brushes on the silicon-supported mixed tris(TMS)/α-bromoisobutyrate monolayer. In comparison with a clean substrate, the modified surfaces bearing

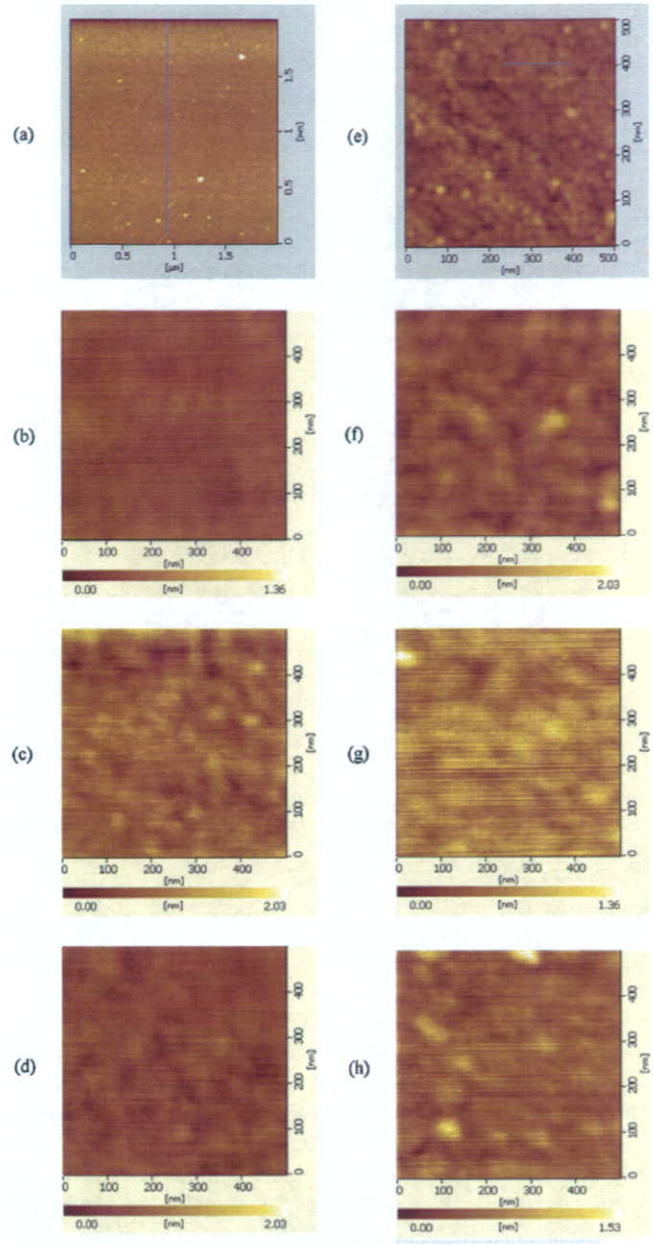

Fig. 8. AFM images of the silicon-supported mixed tris(TMS)/silanol monolayer having varied %tris(TMS) coverage: (a) 0, (b) 51, (c) 66, and (d) 82% and the silicon-supported mixed tris(TMS)/α-bromoisobutyrate monolayer having varied %tris(TMS) coverage: (e) 0, (f) 51, (g) 66, and (h) 82%.

a tris(TMS)/silanol monolayer were almost featureless and relatively smooth (Fig. 8). Average roughnesses (R_a) of all modified substrates are listed in Table 3. Evidently, the coverage of neither tris(TMS) alone nor the tris(TMS) and α-bromoisobutyrate significantly altered overall surface roughness. In order to investigate the spatial distribution of PMPC brushes, the silicon-supported mixed tris(TMS)/silanol surfaces having various percentages of the tris(TMS) coverage were used as nanoscale templates for surface-initiated polymerization. The graft density of surface-tethered α-bromoisobutyrate groups was also varied as a function of reaction time between

Table 3
Average roughness (R_a) of the silicon-supported mixed surfaces determined by AFM analysis

%tris(TMS) coverage	R_a (nm)	
	Silicon-supported mixed tris(TMS)/silanol monolayer	Silicon-supported mixed tris(TMS)/α-bromoisobutyrate monolayer
0	0.2006	0.1708
51	0.0794	0.1322
66	0.1174	0.1401
82	0.0954	0.1508

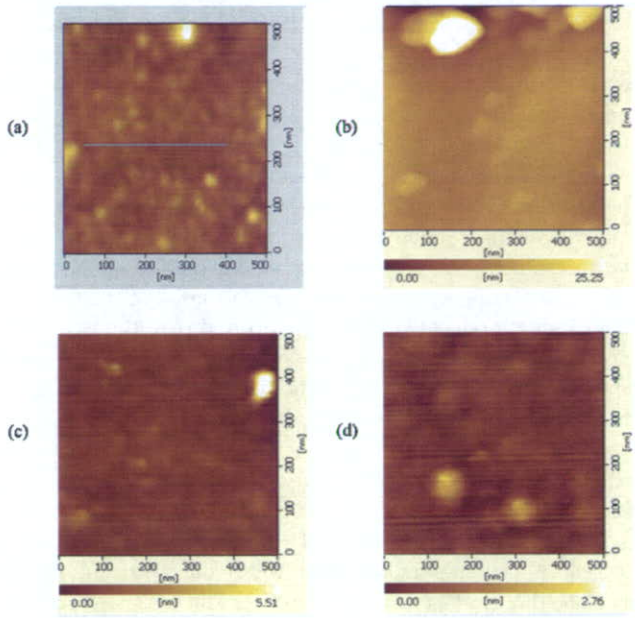

Fig. 9. AFM images of the silicon-supported mixed tris(TMS)/PMPC brushes having varied %tris(TMS) coverage: (a) 0, (b) 51, (c) 66, and (d) 82%.

the residual silanol groups in nanopores with the silane compound having end-functionalized α-bromoisobutyrate groups (n_3).

First, an effect of %tris(TMS) coverage on topography of surfaces having grafted PMPC brushes was explored. Using 96 h of reaction time between the silicon-supported mixed tris(TMS)/silanol monolayers and the silane compound, it was assumed that the residual silanols in nanopores are completely replaced by the α-bromoisobutyrate groups that are capable of initiating polymerization. In other words, the nanopores are mostly filled with surface-tethered initiator and there was not much space between the grafted initiators and the surrounding tris(TMS) groups. Originally, we envisioned that protrusions representing the aggregates of PMPC brushes in the nanopores should appear on the surface and the higher the %tris(TMS) coverage, the smaller the size of protrusions. AFM images of the silicon-supported mixed tris(TMS)/PMPC brushes having different %tris(TMS) coverage using the polymerization time of 1 h, shown in Fig. 9, suggest otherwise. None of the surfaces showed any features that could be evidence of a nanoscopic distribution of PMPC brushes grown from the nanopores, even

Table 4
Average roughness (R_a) of the silicon-supported mixed tris(TMS)/PMPC brushes determined by AFM analysis

%tris(TMS) coverage	R_a (nm)	
	Polymerization time of 1 h	Polymerization time of 5 h
0	0.1783	0.1322
51	0.4660	0.1598
66	0.2359	0.1727
82	0.1398	0.1404

though the silicon-supported mixed tris(TMS)/PMPC brushes having 51% tris(TMS) coverage exhibit higher roughness than the others. According to the data in Table 4, the surfaces became even smoother after a longer period of polymerization (5 h) was used.

We postulate that the densely grafted PMPC brushes within the limited space in the nanopores may be forced by the surrounding tris(TMS) to stretch away from the surface when the polymer chain is relatively short and densely packed inside the nanopores. After a sufficiently long period of polymerization, the polymer chains became so long that they can no longer stretch out, thereby tending to fold over the tris(TMS) monolayer. For that reason, the surface assumes a relatively smooth topography in spite of its low overall graft density in the presence of tris(TMS). That was exactly observed in Fig. 9. Nonetheless, the surfaces may become increasingly rougher if extensive growth of polymer brushes is allowed (polymerization time >5 h).

To visualize the evolution of PMPC brushes grown from nanopores, two alternative routes were undertaken in order to regulate the graft density of PMPC brushes. First, by fixing %tris(TMS) coverage at 82%, one strategy exploited the kinetic control over the reaction between the silicon-supported mixed tris(TMS)/silanol monolayers and the silane compound from 24 to 96 h, which later yielded a low to high graft density of initiator and corresponding PMPC brushes. According to Fig. 10, it was found that the surfaces having varied graft density of PMPC brushes exhibited protrusions having a diameter of less than 100 nm. The size of the protrusions was in good agreement with the average roughness (R_a) listed under each image. The protrusions are believed to represent self-aggregation of PMPC brushes in nanopores. In the case of a low graft density (Fig. 11), there should be enough space within the pores for the polymer chains to adopt a more coil-like architecture or aggregated form (mushroom regime) instead of being in extended forms (brush regime), which are thermodynamically unfavorable. As the packing of PMPC brushes was denser, the protrusions became larger and so did the roughness. The phase separation that led to the PMPC brushes aggregation was believed to be further driven by the different hydrophilicity/hydrophobicity between the PMPC brushes and the surrounding tris(TMS).

Assuming that there is no lateral broadening due to the AFM tip shape, the average number of chains within one of the protrusion can be estimated. First, the volume occupied by one PMPC chain (V_{mol}) was determined using the following equation:

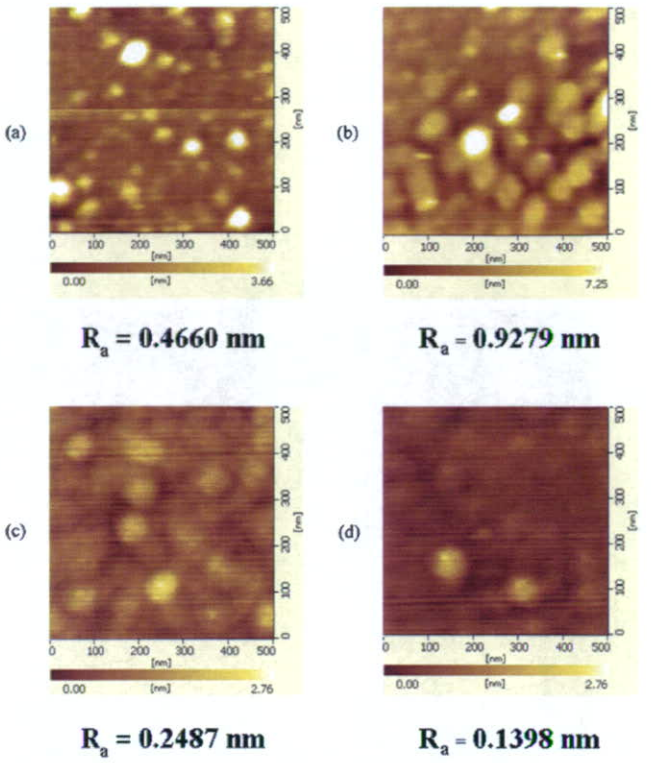

Fig. 10. AFM images of the silicon-supported mixed 82% tris(TMS)/PMPC brushes, controlling the grafting time of initiator: (a) 24, (b) 48, (c) 72, and (d) 96 h.

$$V_{mol} = \frac{M}{\rho N_A}, \tag{4}$$

where the bulk density (ρ) of PMPC is 1.30 g/cm^3 and N_A is the Avogadro number. Using the polymerization time of 1 h and the MPC:added initiator of 200:1, the PMPC molecular weight obtained by GPC analysis is 24,248 g/mol and the calculated V_{mol} is 31 nm^3. From the diameters (d) of the protrusions seen in Figs. 10a–10c which is varied in the range of 30–80 nm, the average volume of the protrusion (V) assuming the shape of a cylindrical disk can be calculated by

$$V = \frac{\pi d^2 h}{4}, \tag{5}$$

where h is the height of the protrusion. The height estimated from AFM image (data not shown) is 1.0 and 1.5 nm for the protrusion having the diameter of 30 and 80 nm, respectively. It turns out that the average volume of the observed protrusions is between 7.1×10^2 and 7.5×10^3 nm^3 which correspond to 23–242 chains. Having the same tris(TMS) coverage (~80%), Stafford and co-workers [27] can only incorporate 5 chains of PS–COOH in the nanopores. These numbers are reasonable considering the fact that we used the "grafting from" method as opposed to their "grafting to" method. To calculate the surface density of the protrusions, the number of chains was divided by the area of the protrusion ($\pi(d/2)^2$). The surface density of the protrusion within the nanopores is varied in the range of 0.02–0.05 chains/nm^2. As expected, these values are well below the

Fig. 11. Schematic representation of possible orientation of PMPC brushes grown from nanopores having different graft density.

densely grafted PMPC obtained under the same polymerization condition which is 0.46 chains/nm^2. This can be explained from the fact that the graft density of the initiator was intentionally kept low in order to avoid a complete filling of the initiator and leave some space for the polymer brush to aggregate in the nanopores. In other words, the number of grafted chains for the high graft density (0.46 chains/nm^2) should be approximately 9–23 times higher than that for the low graft density (0.02–0.05 chains/nm^2) (see Fig. 11).

The surfaces whose nanopores were almost completely covered with PMPC brushes were quite smooth and the protrusions simultaneously diminished, as can be observed in Figs. 10c and 10d. Such behavior might stem from the fact that PMPC brushes were dense enough to be able to fill the nanopores and to eliminate the valley-and-hill features on the surface. The disappearance of the protrusions may be facilitated by two possible actions of polymer brushes previously addressed. The first action involves the polymer chains being forced to stretch away from the surface and thus covering the nanopores while the other involves the folding of polymer chains over the tris(TMS) layer. This latter action should be favorable only when the polymer chains are sufficiently long. The behavior of PMPC brushes is schematically displayed in Fig. 11.

Since the density of PMPC brushes in nanopores is the key to the ability to visualize the polymer distribution, the second alternative route was then performed by varying the %tris(TMS) coverage but fixing the graft density of the initiator at a low value by using a short reaction time (24 h) between the silicon-supported mixed tris(TMS)/silanol monolayers and the silane compound. These experiments were designed in order to make sure that the residual silanols in nanopores were not completely replaced by the α-bromoisobutyrate groups and that there was some space between the grafted PMPC brushes and the surrounding tris(TMS). After the formation of polymer brushes, there should be some space for PMPC brushes to aggregate inside the nanopores. AFM images of the silicon-supported mixed tris(TMS)/PMPC brushes prepared by this approach using a 1 h polymerization time are illustrated in Fig. 12. The size of protrusions obviously reflected the size of nanopores, which should be inversely proportional to %tris(TMS) coverage. The higher the %tris(TMS) coverage, the smaller the protrusions.

A comparative investigation has been conducted on the system of the silicon-supported mixed tris(TMS)/P*t*-BMA brushes. Fig. 13 shows AFM images of the silicon-supported mixed tris(TMS)/P*t*-BMA brushes having 82% tris(TMS) coverage. P*t*-BMA brushes were grown for 1 h from the silicon-supported mixed tris(TMS)/α-bromoisobutyrate having different graft densities of α-bromoisobutyrate groups. Conducting the reaction between the silicon-supported mixed tris(TMS)/silanol monolayers and silane compound having

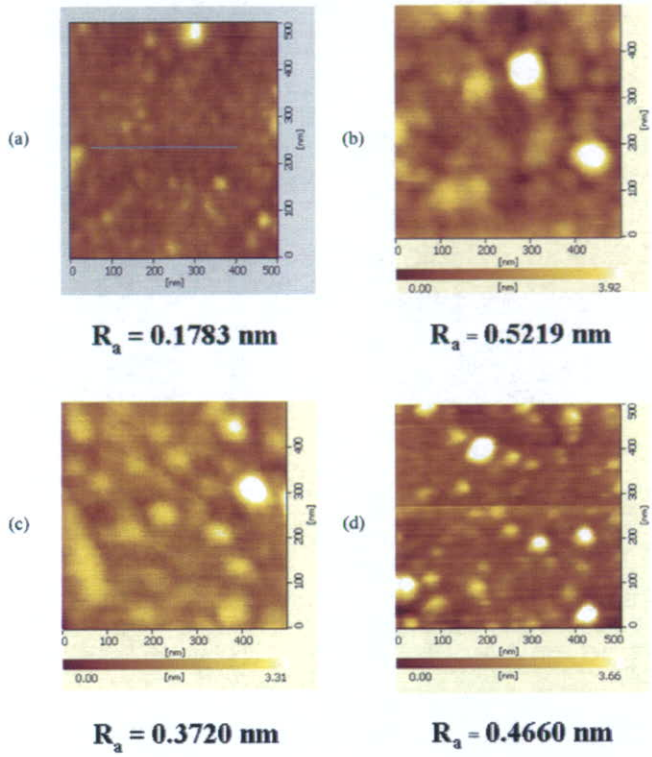

Fig. 12. AFM images of the silicon-supported mixed tris(TMS)/PMPC brushes using grafting time of initiator as 24 h and varied % tris(TMS) coverage: (a) 0, (b) 51, (c) 66, and (d) 82%.

end-functionalized α-bromoisobutyrate groups for 24 and 96 h yielded a low and high graft density of α-bromoisobutyrate groups, respectively. Even though both surfaces (Figs. 13a and 13b) have different graft densities of P*t*-BMA brushes, their surface topographies are indistinguishable and relatively smooth in texture. The surfaces became rougher when the polymerization time was extended from 1 to 5 h without affecting surface topographies (Figs. 13c and 13d). Unlike PMPC brushes, P*t*-BMA brushes are hydrophobic. Therefore, they should be quite miscible with tris(TMS). In fact, this speculation can be confirmed by the contact angle data shown in Fig. 5. The mixed tris(TMS)/P*t*-BMA brush system thereby did not exhibit nanoscopic phase separation although the surface graft density of P*t*-BMA brushes was low. These results also imply that self-aggregation of PMPC brushes in nanopores, which leads to protrusions, is truly a consequence of phase incompatibility between hydrophilic PMPC brushes and hydrophobic tris(TMS). Once again, it should be highlighted that such nanoscopic phase separation was noticeable when the graft density of PMPC brushes was low. This observation is, however, in contrast to the previous work reported by Stafford et al. [27].

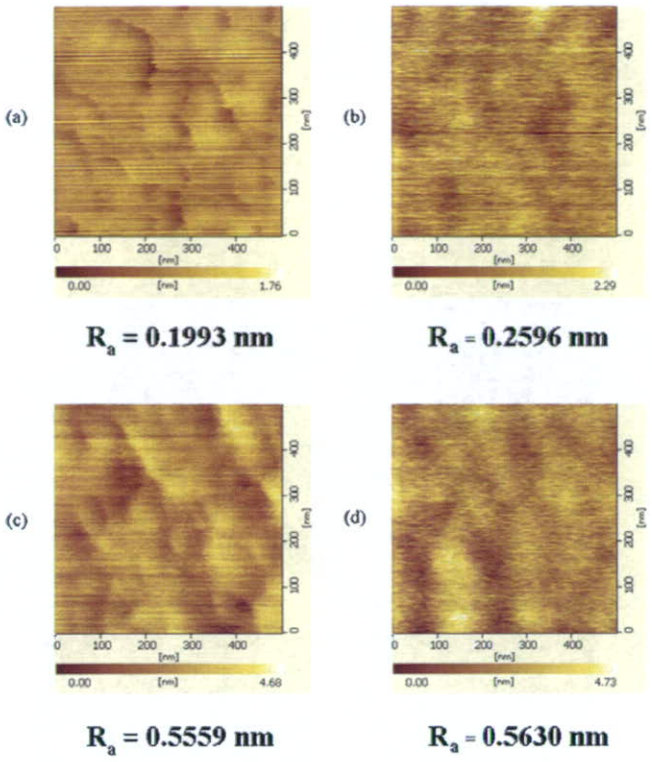

Fig. 13. AFM images of the silicon-supported mixed 82% tris(TMS)/P*t*-BMA brushes, controlling the grafting time of initiator (t_i) and polymerization time (t_p): (a) $t_i = 24$ h, $t_p = 1$ h, (b) $t_i = 96$ h, $t_p = 1$ h, (c) $t_i = 24$ h, $t_p = 5$ h, and (d) $t_i = 96$ h, $t_p = 5$ h.

Despite the hydrophobicity of polystyrene ($\theta_A/\theta_R = 95°/79°$), the nanoscopic distribution of polystyrene aggregates was observed after the adsorption of carboxyl-terminated polystyrene on the nanoporous tris(TMS)/silanol monolayers. The dimension of aggregates corresponded very well with the %tris(TMS) coverage. We believe the following reasons account for such difference. As opposed to our "grafting from" approach, the "grafting to" approach, used in their study, should suffer an entropic barrier due to crowding of initial grafting polymer chains that prevent further insertion of polymer onto the surface. As a result, the graft density should be extremely low (lower than our P*t*-BMA brushes), especially when the "grafting to" was done on the nanoporous surface. Based on their calculation, as few as one polystyrene chain was grafted in the nanopore of the surface having relatively high tris(TMS) coverage. The coil-like conformation should thus be more favorable than the extended one, leading to the aggregation of the end-grafted polystyrene regardless of its comparable hydrophobicity with the tris (TMS).

3.5. Anti-fouling characteristics of PMPC brushes in nanopores

As a biocompatible polymer, PMPC is well recognized for its anti-fouling characteristic, meaning it resists non-specific interactions with plasma proteins and cells. One way to test the effect of the nanoscopic spatial distribution of PMPC brushes on the surface property is to determine the interactions between the silicon-supported mixed tris(TMS)/PMPC brushes having different %tris(TMS) coverage with plasma proteins. The protein adsorption data are summarized in Table 5. Due to the hydrophilic nature of the silicon substrate, the amount of protein adsorption was quite low. The amount of adsorbed protein slightly increased on a more hydrophobic silicon-supported α-bromoisobutyrate monolayer. Even though the amount of plasma protein adsorbed on the surfaces having PMPC brushes was lower than that on the surface grafted with α-bromoisobutyrate, the difference was not that significant considering the more hydrophilic nature of PMPC in comparison with the surface covered with an α-bromoisobutyrate monolayer. In order to verify that the reduction of protein adsorption was really due to the presence of PMPC brushes, P*t*-BMA was chosen as a positive control. The fact that P*t*-BMA brushes adsorbed a greater amount of protein as opposed to PMPC brushes helped confirm the above interpretation.

The amount of protein adsorbed on the surface having PMPC brushes was almost independent of the thickness of polymer brushes, implying that PMPC brushes being as thin as ~1 nm were sufficient to obtain the protein-resistance property. Apparently, the coverage of tris(TMS) played a significant role in controlling protein adsorption. The higher the content of tris(TMS) or the lower the graft density of PMPC brushes on the surface, the higher the quantity of the adsorbed protein. Unlike the silicon-supported PMPC brushes, the response to plasma proteins of the silicon-supported mixed tris(TMS)/PMPC brushes depended upon the thickness of polymer brushes. Considering the series of silicon-supported mixed 66% tris(TMS)/PMPC brushes, it seems that the longer polymer brushes were capable of repelling plasma protein despite their relatively low graft density or high %tris(TMS) coverage.

This outcome is in good agreement with the hypothesis previously proposed based on topographic evidence obtained from AFM analysis. It was postulated that the stretching of long polymer chains is thermodynamically unfavorable so the polymer chains tend to fold over the tris(TMS) monolayer. The lower receding contact angle as a function of polymer thickness can be an indication of PMPC brushes dominating at polymer/water interfaces or under hydrated conditions. As a result, the coverage of PMPC brushes is no longer directly correlated with %tris(TMS). In other words, the protein resistance is no longer dictated by %tris(TMS) but rather by the thickness of PMPC brushes instead.

In the case of homogeneously and densely grafted PMPC brushes grown from the silicon-supported α-bromoisobutyrate monolayer, the protein adsorption does not depend on the thickness of polymer brushes as long as the surface is fully covered by the polymer brushes. The extremely thin layer of polymer brushes is certainly enough for generating a non-fouling surface. On the other hand, the thickness and the graft density of polymer brushes become important parameters in controlling protein adsorption on heterogeneously and loosely grafted PMPC brushes grown from the silicon-supported tris(TMS)α-bromoisobutyrate monolayer. When polymer brushes are quite short, the polymer chains are forced to stretch out or aggregate

Table 5
The amount of plasma protein adsorbed on various silicon substrates

Surface	Thickness of polymer brushes (nm)	Water contact angle (θ_A/θ_R)	Amount of protein adsorbed ($\mu g/cm^2$)
Silicon oxide	–	~0°	0.16 ± 0.06
Silicon-supported α-bromoisobutyrate monolayer	–	71°/62°	0.33 ± 0.15
Silicon-supported PMPC brushes	1.0	23°/0°	0.23 ± 0.05
	2.6	22°/0°	0.20 ± 0.03
	6.4	20°/0°	0.17 ± 0.02
Silicon-supported Pt-BMA brushes	1.8	92°/72°	5.24 ± 0.30
	3.0	94°/77°	6.20 ± 0.20
Silicon-supported mixed 66% tris(TMS)/PMPC brushes	2.6	56°/30°	1.70 ± 0.17
	3.0	54°/27°	0.62 ± 0.05
	4.3	54°/20°	40.07 ± 0.03
Silicon-supported mixed 75% tris(TMS)/PMPC brushes	2.3	63°/31°	2.71 ± 0.09
Silicon-supported mixed 82% tris(TMS)/PMPC brushes	1.8	70°/40°	3.92 ± 0.27

in the nanopores surrounded by tris(TMS), so the protein adsorption varies as a function of %tris(TMS) or the graft density of PMPC brushes. In contrast, when the polymer brushes are so long that they can fold and partly cover tris(TMS), the protein adsorption no longer relies on %tris(TMS), but is mainly influenced by the length or the thickness of the polymer brushes. Our results are in good agreement with the data previously reported by Feng et al. [38]. They have observed that PMPC chains were very effective in preventing protein adsorption even with the short chain lengths (low thickness) at the high graft density. They have therefore concluded that graft density is more important than the chain length for preventing protein adsorption.

4. Conclusions

The incomplete reaction between the sluggish tris(TMSCl) and silicon oxide surface allowed silicon-supported mixed tris(TMS)/silanol monolayers having a range of tris(TMS) coverage to be formed. Nanoscale holes (nanopores) in tris(TMS) monolayers containing unreacted silanol groups of silicon-supported mixed tris(TMS)/silanol monolayers further reacted with silane compounds having end-functionalized α-bromoisobutyrate and yielded silicon-supported mixed tris(TMS)/α-bromoisobutyrate monolayers. PMPC brushes grew faster from surface-immobilized α-bromoisobutyrate initiators having hexyl (n_6) and decyl (n_{10}) as alkyl spacers in comparison with propyl (n_3) as an alkyl spacer. The better mobility and the longer alkyl spacers of n_6 and n_{10} allowed them to overcome the steric hindrance of the surrounding tris(TMS) and reach monomers more efficiently than n_3.

The nanoscopic distribution of PMPC brushes, which appeared as protrusions having a diameter of less than 100 nm, was only visualized when the graft density of PMPC brushes in the nanopores was not too high. Under such circumstances, the size of protrusions depended upon both the %tris(TMS) coverage as well as the graft density of PMPC brushes itself in the nanopores. In the case of a high graft density of PMPC brushes in the nanopores, the surfaces became quite smooth due to the polymer chains being forced to stretch away from the surface, thus covering the nanopores, and the folding of polymer chains over the tris(TMS) layer when the polymer chains are sufficiently long. Unlike PMPC brushes, Pt-BMA brushes are hydrophobic so they should be quite compatible with tris(TMS). The mixed tris(TMS)/Pt-BMA brush system thereby did not exhibit nanoscopic phase separation although the graft density of Pt-BMA brushes in the nanopores was quite low. These results also implied that self-aggregation of PMPC brushes in the nanopores was truly a consequence of phase incompatibility between hydrophilic PMPC brushes and hydrophobic tris(TMS). The protein adsorption studies have demonstrated that the antifouling characteristic, a key surface property of PMPC brushes, is influenced by the percentage of tris(TMS) as well as the chain length of the polymer brushes.

Acknowledgments

This research is supported by the Thailand Research Fund (TRG4580049), a TJTTP-JBIC project (under the Center for Bioactive Compounds, Chulalongkorn University) and a graduate research grant for Mayuree Srinanthakul from Chulalongkorn University. The authors are grateful to the Capability Building Unit for Nanoscience and Nanotechnology, Mahidol University and the Electronic Research Center, Faculty of Engineering, King Mongkut's Institute of Technology, Ladkrabang for providing Atomic Force Microscopy and Ellipsometry facilities, respectively. Appreciation is also extended to the National Metal and Materials Technology Center (MTEC) for providing the contact angle goniometer.

References

[1] S.T. Milner, Science 251 (1991) 905.
[2] A. Halperin, M. Tirrell, T.P. Lodge, Adv. Polym. Sci. 100 (1992) 31.
[3] B. Zhao, W.J. Brittain, Prog. Polym. Sci. 25 (2000) 677.
[4] Y. Ito, Y. Ochiai, Y.S. Park, Y. Imanishi, J. Am. Chem. Soc. 119 (1997) 1619.

[5] Y.S. Park, Y. Ito, Y. Imanishi, Macromolecules 31 (1998) 2606.
[6] O. Prucker, J. Rühe, Macromolecules 31 (1998) 592.
[7] X. Huang, M.J. Wirth, Macromolecules 32 (1999) 1694.
[8] K. Matyjaszewski, P.J. Miller, N. Shukla, B. Immaraporn, A. Gelman, B.B. Luokala, T.M. Siclovan, G. Kickelbick, T. Vallant, H. Hoffman, T. Pakula, Macromolecules 32 (1999) 8716.
[9] J.B. Kim, M.L. Bruening, G.L. Baker, J. Am. Chem. Soc. 122 (2000) 7616.
[10] B. Zhao, W.J. Brittain, Macromolecules 33 (2000) 8813.
[11] M. Ejaz, K. Ohno, Y. Tsuji, T. Fukuda, Macromolecules 33 (2000) 2870.
[12] T. von Werne, T.E. Patten, J. Am. Chem. Soc. 123 (2001) 7497.
[13] M. Husseman, E.E. Malmstrom, M. McNamara, M. Mate, D. Mecerreyes, D.G. Benoit, J.L. Hedrick, P. Mansky, E. Huang, T.P. Russell, C.J. Hawker, Macromolecules 32 (1999) 1424.
[14] H. Mori, A. Böker, G. Krausch, A.H.E. Müller, Macromolecules 34 (2001) 6871.
[15] M. Khan, W.T.S. Huck, Macromolecules 36 (2003) 5088.
[16] J. Rühe, Macromol. Symp. 126 (1998) 215.
[17] G.P. Chen, Y. Ito, Y. Imanishi, Macromolecules 30 (1997) 7001.
[18] M. Husemann, M. Morrison, D. Benoit, K.J. Frommer, C.M. Mate, W.D. Hinsberg, J.L. Hedrick, C.J. Hawker, J. Am. Chem. Soc. 122 (2000) 1844.
[19] J. Aizenberg, A.J. Black, G.M. Whitesides, Nature 394 (1998) 868.
[20] A.J. Black, K.E. Paul, J. Aizenberg, G.M. Whitesides, J. Am. Chem. Soc. 121 (1999) 8356.
[21] M. Husemann, D. Mercerreyes, C.J. Hawker, J.L. Hedrick, R. Shah, N.L. Abbott, Angew. Chem. Int. Ed. 38 (1999) 647.
[22] R.R. Shah, D. Merreceyes, M. Husemann, I. Rees, N.L. Abbott, C.J. Hawker, J.L. Hedrick, Macromolecules 33 (2000) 597.
[23] L. Yan, W.T.S. Huck, X.M. Zhao, G.M. Whitesides, Langmuir 15 (1999) 1208.
[24] R.W. Zehner, L.R. Sita, Langmuir 15 (1999) 6139.
[25] D. Mecerreyes, E. Huang, T. Magbitang, W. Volksen, C.J. Hawker, V.Y. Lee, R.D. Miller, J.L. Hedrick, High Perform. Polym. 13 (2001) S11.
[26] A.Y. Fadeev, T.J. McCarthy, Langmuir 15 (1999) 7238.
[27] C.M. Stafford, A.Y. Fadeev, T.P. Russell, T.J. McCarthy, Langmuir 17 (2001) 6547.
[28] X. Jia, T.J. McCarthy, Langmuir 19 (2003) 2449.
[29] J.N. Israelachvili, M.L. Gee, Langmuir 5 (1989) 288.
[30] K. Ishihara, H. Oshida, Y. Endo, A. Watanabe, T. Ueda, N. Nakabayashi, J. Biomed. Mater. Res. 27 (1993) 1309.
[31] K. Ishihara, H. Nomura, T. Mihara, K. Kurita, Y. Iwasaki, N. Nakabayashi, J. Biomed. Mater. Res. 39 (1998) 323.
[32] Y. Iwasaki, S. Sawada, K. Ishihara, G. Khang, H.B. Lee, Biomaterials 23 (2002) 3897.
[33] S. Sawada, S. Sakaki, Y. Iwasaki, N. Nakabayashi, K. Ishihara, J. Biomed. Mater. Res. A 64 (2003) 411.
[34] X.Y. Chen, S.P. Armes, Adv. Mater. 15 (2003) 1558.
[35] W. Feng, J. Brash, S.P. Zhu, J. Polym. Sci. Polym. Chem. 42 (2004) 2931.
[36] R. Iwata, P. Suk-in, V.P. Hoven, A. Takahara, K. Akiyoshi, Y. Iwasaki, Biomacromolecules 5 (2004) 2308.
[37] W. Feng, S.P. Zhu, K. Ishihara, J.L. Brash, Langmuir 21 (2005) 5980.
[38] W. Feng, J.L. Brash, S.P. Zhu, Biomaterials 27 (2006) 847.
[39] S. Heid, F. Effenberger, K. Bierbaum, M. Grunze, Langmuir 12 (1996) 2118.
[40] M. Ejaz, Y. Tsujii, T. Fukuda, Polymer 42 (2001) 6811.

Selective Biorecognition and Preservation of Cell Function on Carbohydrate-Immobilized Phosphorylcholine Polymers

Yasuhiko Iwasaki,*,†,‡ Utae Takami,‡,§ Yurika Shinohara,‡,§ Kimio Kurita,§ and Kazunari Akiyoshi‡,∥

Department of Chemistry and Materials Engineering, Faculty of Chemistry, Materials and Bioengineering, Kansai University, 3-3-35 Yamate-cho, Suita-shi, Osaka 564-8680, Japan, Institute of Biomaterials and Bioengineering and Center of Excellence Program for Frontier Research on Molecular Destruction and Reconstruction of Tooth and Bone, Tokyo Medical and Dental University, 2-3-10 Kanda-surugadai, Chiyoda-ku, Tokyo 101-0062, Japan, and Department of Materials and Applied Chemistry, College of Science and Technology, Nihon University, 1-8-14 Kanda-surugadai, Chiyoda-ku, Tokyo 101-8308, Japan

Received April 30, 2007; Revised Manuscript Received June 13, 2007

To obtain synthetic materials capable of selectively recognizing proteins and cells, and preserving their functions, biomembrane mimetic polymers having a phospholipid polar group and carbohydrate side chains were designed. Poly[2-methacryloyloxyethyl phosphorylcholine (MPC)-*co*-*n*-butyl methacrylate (BMA)-*co*-2-lactobionamidoethyl methacrylate (LAMA)] (PMBL) was synthesized and coated on substrates by solvent evaporation. Selective binding of galactose-recognized lectin, RCA_{120}, to a PMBL surface was investigated by measurement of surface plasmon resonance. The binding of RCA_{120} to the PMBL surface was confirmed by a remarkable change in resonance angle. The apparent affinity constant of RCA_{120} to PMBL3.0 (3.0 mol % LAMA unit in the feed) per LAMA unit was $2.77 \times 10^5\ M^{-1}$. When a glucose-recognized lectin, concanavalin A, was in contact with PMBL, no change in the resonance angle was observed, and any nonspecific fouling of protein on PMBL was effectively reduced. Cells of the human hepatocellular liver carcinoma cell line (HepG2) having asialoglycoprotein receptors (ASGPRs) were seeded on polymer surfaces. On poly(BMA) (PBMA), many adherent cells were observed and were well-spread with monolayer adhesion, but cell adhesion was reduced on poly(MPC-*co*-BMA) (PMB). HepG2 adhesion was observed on PMBL because the cell has ASGPRs; the number of cells adhering to the PMBL polymer surfaces increased with an increase in the density of galactose residues on the surface. In contrast, adhesion of NIH-3T3 cells to PMBL was reduced in a manner similar to that on PMB because the NIH-3T3 cells did not have ASGPRs. Cell adhesion to the PMBL surface was well-regulated by ligand−receptor interactions. Furthermore, some of the cells adhering to the PMBL surface had a spheroid form, and similarly shaped spheroids were scattered on the surface. Although poly(BMA-*co*-LAMA) (PBL) has galactose residues, the adherent cells were spread in a manner similar to those on PBMA. The MPC units in PMBL contribute to make a spheroid formation of HepG2 cells. The amount of albumin secreted from a cell was compared with the chemical structure of the substrate. The spheroid shaped cells cultured on the PMBL surface secreted much more albumin than did the spreading cells that adhered to the PBMA. In conclusion, the biomembrane mimetic carbohydrate-immobilized phosphorylcholine polymers produced a suitable surface for biorecognition and preservation of cell function.

Introduction

Control of cell adhesion and the function of synthetic polymers are important in molecular separation, biosensors, and development of biomedical materials.[1,2] In this article, we explore the ability of biomembrane mimetic polymer surfaces to recognize specific biosubstances from their physiological conditions.

Using physicochemical and biological approaches, various surface conditions, such as a wettability gradient,[3] topological patterns,[4,5] peptide immobilization,[6−13] and carbohydrates[14−20] have been applied to control cell attachment. The physicochemical or topological systems enable control of the surface density of adherent cells, but these surfaces cannot recognize the specific type of cell. By ligand immobilization on a synthetic surface, recognition selectivity could be improved. Arg−Gly−Asp (RGD) immobilized surfaces have been studied extensively to induce cell adhesion based on ligand−receptor interactions.[6,11−13] While these approaches improved cell adhesion, the selectivity of RGD is limited because the RGD sequence is not unique for a specific cell. The immobilization was generally performed on conventional polymers, and nonspecific interactions occurred between the cell and the synthetic surface.

Carbohydrates are also one of the most reliable candidates as ligands immobilized on a surface because carbohydrates on a cell surface contribute to most forms of communication between living cells and their environment.[16] In particular, galactose residues are preferably conjugated polymers to interact with hepatocytes, which are asialoglycoprotein receptors (ASGPRs). The ASGPR is a lectin for receptor-mediated endocytosis found at the hepatocyte cell surface, which is bound to galactose/*N*-acetylgalactosamine (GalNAc)-terminated ligands

* Corresponding author. Tel.: +81-6-6368-0090; fax: +81-6-6368-0090; e-mail: yasu.bmt@ipcku.kansai-u.ac.jp.

† Kansai University.

‡ Institute of Biomaterials and Bioengineering, Tokyo Medical and Dental University.

§ Nihon University.

∥ Center of Excellence Program for Frontier Research on Molecular Destruction and Reconstruction of Tooth and Bone, Tokyo Medical and Dental University.

10.1021/bm700478d CCC: $37.00
Published on Web 07/31/2007

Table 1. Synthetic Results and Surface Characterization of PMBL

	molar fraction (MPC/BMA/LAMA)				XPS elemental data (%)[a]			
abbreviation	in feed[b]	in copolymer[c]	M_w (10^5)	M_w/M_n	C	O	N	P
PMBL0.5	0.200/0.795/0.005	0.192/0.801/0.006	4.7	2.1	71.4	25.1	1.3	2.2
					(72.8)	(23.9)	(1.7)	(1.6)
PMBL1.0	0.200/0.790/0.010	0.172/0.817/0.011	3.7	1.7	70.5	25.3	1.8	2.4
					(73.2)	(23.8)	(1.6)	(1.5)
PMBL3.0	0.200/0.770/0.030	0.180/0.801/0.019	3.4	1.8	70.2	26.5	1.6	1.7
					(72.5)	(24.3)	(1.7)	(1.5)
PMB	0.300/0.700/−	0.314/0.686/−	7.4	1.8	71.0	25.2	1.3	2.5
					(69.7)	(25.4)	(2.4)	(2.4)
PBL1.0	−/0.990/0.010	−/0.992/0.008	2.4	1.5	−	−	−	−
					(79.4)	(20.5)	(0.1)	(−)

[a] Takeoff angle = 90°. Theoretical elemental data calculated from bulk concentration are in parentheses. [b] [Monomer] = 1.0 M, [AIBN] = 5 mM, temperature = 60 °C, and solvent is EtOH/DMSO. [c] Determined by phosphorus analysis and anthrone sulfuric acid method.

in a calcium-dependent manner.[17,18] Although the ASGPR does not function physiologically as an adhesion receptor, galactose-containing polymers have been used to induce adhesion in primary hepatocytes.[19−21] Various polymers bearing galactose residues as ligands were prepared for drug delivery[22] and cellular matrices.[23] While these approaches have been quite successful, limitations remain in terms of selective recognition.[24] Indeed, most earlier reports did not focus on the reduction of nonspecific interactions.

We have been studying 2-methacryloyloxyethyl phosphorylcholine (MPC) polymers synthesized as biomimetics of phospholipids in a biomembrane.[25−28] MPC polymers have a surface that resists nonspecific protein adsorption and cell adhesion (i.e., biofouling).[29,30] Biofouling reduces the functionality of a material and can induce an unexpected bioreaction. Further, it has been shown that cells in contact with MPC polymers do not exhibit activation or an inflammatory response.[31,32] Although nonfouling phenomena of MPC polymer surfaces have been extensively studied, carbohydrate-immobilized MPC polymers have not been synthesized for creating biorecognition surfaces.

We hypothesized that MPC polymer surfaces bearing carbohydrates might perform in the same way as biomembrane mimetic surfaces, which can interact with a specific cell and control its function. In this study, an MPC copolymer with galactose residues has been synthesized for the first time, and we present here the effectiveness of the surface in controlling cell−material interactions and preserving cell function.

Materials and Methods

Polymer Synthesis. *n*-Butyl methacrylate (BMA) was purified by conventional distillation. MPC was synthesized as previously reported.[33] 2-Lactobionamidoethyl methacrylate (LAMA) was synthesized by reacting lactobionolactone and 2-aminoethyl methacrylate hydrochloride.[34] Other reagents and solvents were obtained commercially in extra-pure grade and used without further purification.

Poly(MPC-*co*-BMA) (PMB), poly(BMA-*co*-LAMA) (PBL), and poly(MPC-*co*-BMA-*co*-LAMA) (PMBL) were synthesized by conventional radical polymerization using 2,2′-azobisisobutyronitrile (AIBN) as an initiator. BMA was used as a comonomer because it enables the processing of a polymer membrane. The mole fraction of the MPC and LAMA units in the polymer was determined by phosphorus analysis and the anthrone sulfate method, respectively. The number-averaged and weight-averaged molecular weights of the polymers were determined with a Tosoh gel permeation chromatography (GPC) system with a refractive index detector and size exclusion columns (Polymer Laboratories Ltd.) and MIXED-C with a poly(methyl methacrylate) standard (PMMA, Tosoh standard sample) in $CHCl_3$ or $CHCl_3$/methanol (6:4, vol/vol). The results of polymerization are summarized in Table 1.

Preparation of Sample Plates for Cell Culture Experiments. Poly(ethylene terephthalate) (PET) plates (14 mm in diameter; Wako Pure Chemical Industries, Ltd.) were immersed in an ethanol or toluene solution of the polymer (0.5 wt %) and dried under a vapor atmosphere of the solvent at room temperature for 30 min. This procedure was repeated twice, after which the plates were dried in vacuo. The surface properties of the polymer-coated PET plates were analyzed by surface contact angle measurement (G-1, Erma) and X-ray photoelectron spectroscopy (XPS; Kratos-Shimazu) with a magnesium anode (takeoff angle of 90°). Survey scan spectra of C_{1s}, O_{1s}, N_{1s}, and P_{2p} were taken.

Selective Binding of Lectins on Polymer Surfaces. The binding of lectins on the polymer surfaces was determined by asurface plasmon resonance (SPR; Moritex) sensor. Gold-spattered sensor chips were purchased from Moritex, and the polymers were further coated using a spin coater (ACT-220A, ACTIVE Co., Ltd.) at 4000 rpm from a 0.25 wt % solution. The running buffer for the SPR was a phosphate buffered solution (PBS; 150 mM sodium chloride, pH 7.4). Galactose-recognizing lectin (RCA_{120}; Vector Laboratories, Inc.) or glucose binding lectin, concanavalin A (Con A; Vector Laboratories, Inc.), was in contact with the polymer-coated sensor chips. After the lectin solution was in contact with the polymer surfaces for 10 min, the surfaces of the sensor chips were rinsed with running buffer. The change in resonance angle due to the adsorption/desorption of lectin was monitored. Apparent affinity constants per LAMA unit (K_a) and changes in maximum angle ($\Delta\theta_{max}$) were calculated from the slope and intercepts according to Langmuir (eq 1)[35]

$$[\text{lectin}]/\Delta\theta = [\text{lectin}]/\Delta\theta_{max} + 1/\Delta\theta_{max}K_a \quad (1)$$

Cell Culture Experiments. Before the cell culture experiments were performed, protein adsorption on the polymer surfaces from the culture medium was determined because cell adhesion is strongly dependent on protein adsorption. PBMA-, PMBL-, and PBL-coated PET plates were placed in contact with PBS to equilibrate their surfaces. The plates were then soaked in the culture medium (Eagle's MEM; Nissui Pharmaceutical) containing 10% fetal bovine serum (FBS) at 37 °C. The amount of adsorbed proteins on the polymer surfaces from 10% FBS was determined by the micro-BCA method.[36]

Human hepatocellular liver carcinoma cell line (HepG2) cells and mouse fibroblasts (NIH-3T3) were purchased from RIKEN Cell Bank. The cells were maintained in a culture medium containing 10% FBS at 37 °C in a humidified atmosphere of air containing 5% CO_2. For cell maintenance, the contents of the flasks were detached by trypsin treatment. The concentration of the cells was adjusted to 2.0×10^4 cells/mL. The cells (1 mL suspension) were seeded on the polymer surfaces and continuously cultured for specific periods in the CO_2

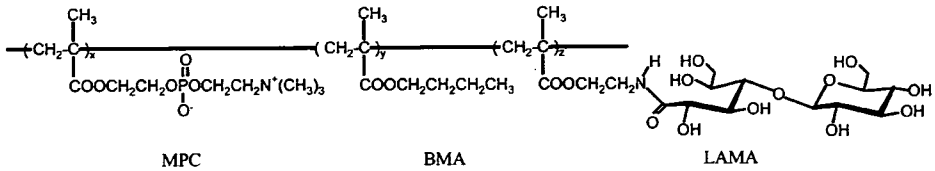

Figure 1. Structure of PMBL.

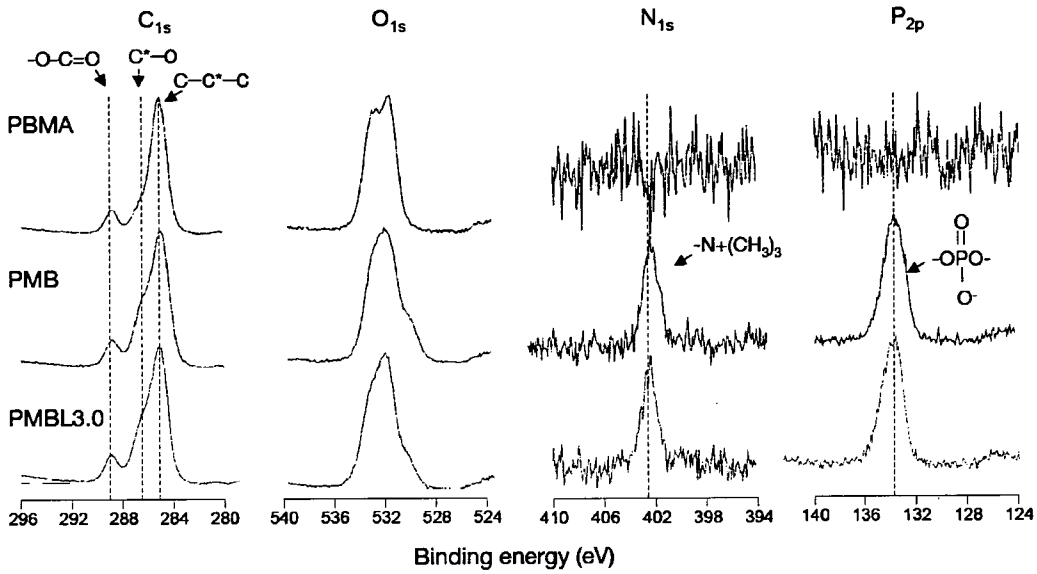

Figure 2. XPS spectra of polymer surfaces.

incubator with 95% humidity. After the cells were incubated on the polymer samples for the specific periods, the polymer plates were rinsed 3 times with PBS. The plates were then transferred to a new 24-well tissue culture plate. Triton X-100 (0.5 wt %, 1 mL) was introduced into each well, and the cells were incubated for 30 min. The Triton X-100 solution (250 μL) was collected, and the concentration of LDH from the adherent cells was measured with an LDH-Cytotoxic Test kit (Wako Pure Chemical Industries, Ltd.).[37,38]

Morphological observation of the HepG2 cells cultured on the polymer surfaces was performed using a confocal laser scanning microscope (LSM510, Zeiss). Cultured cells were fixed at 37 °C with 4% para-formaldehyde in Dulbecco's PBS for 20 min. The fixed surfaces were washed with PBS and permeabilized with 0.5% Triton X-100 in PBS for 2 min. The surfaces were then blocked with 0.1% BSA in PBS for 90 min. To enable observation of the cell membrane, a DMSO solution (10 μL) of 10 μM Texas Red-DHPE (Molecular Probes Inc.) and 0.1% BSA/PBS (1 mL) was poured into each well and stored for 30 min. After being rinsed with 0.1% BSA/PBS (1 mL) 3 times, F-actin synthesized in the cells was stained for assay by immunocytochemistry. The cells were in contact with primary antibodies [anti-human actin goat polyclonal antiserum (Sigma Chemical)], rinsed with PBS, and then incubated with FITC conjugated secondary antibody [FITC conjugated anti-goat IgG rabbit IgG (Sigma Chemical)]. The surfaces were then sufficiently rinsed with 0.1% BSA/PBS after which they were mounted for observation.

Albumin secreted from the HepG2 cells cultured on the polymer surfaces was determined by an enzyme linked immunosorbent assay (ELISA). After the HepG2 cells on the polymer surfaces were cultured for 96, 168, or 360 h, the culture medium was entirely changed, and additional culturing was continued for 24 h. The supernatant of the medium was collected, and the concentration of albumin was determined.

Statistical Analysis. The data are represented as the mean + the standard deviation (SD). Statistical comparisons ($n = 4$) were performed with the Student's t test.

Results and Discussion

Polymer Synthesis. To control biorecognition, polymer surfaces containing phospholipid polar groups and carbohydrates were designed as biomimetics of the outer surface of a biomembrane. Carbohydrate residues were added to the phosphorylcholine polymer surfaces as recognition sites. Figure 1 shows the structures of the polymers synthesized in this study. The polymerization of MPC, BMA, and LAMA was carried out in a DMSO mixture. As indicated in Table 1, the feed could be used to control the composition of each monomer unit. Copolymers containing various amounts of carbohydrate units were thus obtained. PET plates coated with the synthesized polymers from a 0.5 wt % solution were prepared by solvent evaporation. Elemental analysis of polymer-coated PET surfaces was performed by XPS. In the case of the PET plates coated with MPC polymers, nitrogen and phosphorus peaks were observed at 402.5 and 133.0 eV, respectively (Figure 2). O_{1s} shows a low binding energy component around 530 eV, which is most probably due to the PO_4 environment in phosphorylcholine. The XPS elemental concentration was summarized in Table 1. The concentration of oxygen was slightly increased by the addition of the LAMA unit to the copolymer. This increase is due to the hydroxyl groups of the carbohydrates and the LAMA units located on the surface of the sample plates.

Selective Binding of Lectin on Polymer Surfaces. To identify the selective interaction of lectin on the PMBL surface, the binding behavior was monitored by SPR. Figure 3 shows time courses of the change in the resonance angle of SPR responding to the addition of RCA_{120} to a PMBL3.0-coated gold surface in PBS (pH 7.4). The change in the resonance angle ($\Delta\theta$) due to RCA_{120} binding to PMBL3.0 was remarkable and well-correlated with the concentration of RCA_{120}. The apparent binding constant of RCA_{120} to PMBL3.0 per LAMA unit was

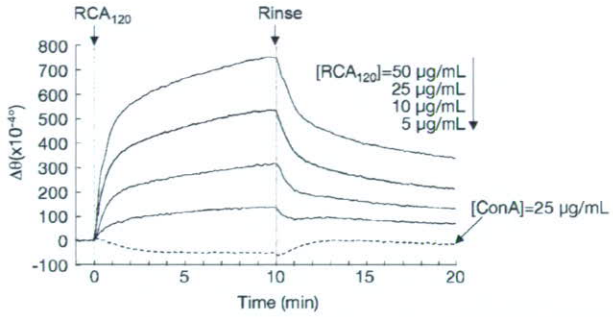

Figure 3. SPR curve on PMBL3.0 after contact with RCA120.

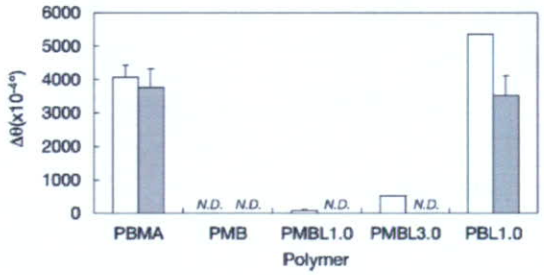

Figure 4. Change in the resonance angle of polymer-coated SPR sensors after contact with lectin for 10 min: (white) RCA_{120} and (gray) Con A.

$2.77 \times 10^5\ M^{-1}$. Because these values are comparable to the affinity constant between the lactose-carrying polymer and RCA_{120}, it can be said that the conjugate is strongly bound to the lectin by the glycocluster effect.[39,40] When Con A was in contact with the PMBL3.0-coated gold surface, the resonance angle was minimally changed, as shown in Figure 3. The $\Delta\theta$ value of various SPR sensor-coated polymers due to lectin binding is summarized in Figure 4. On PBMA and PBL1.0, $\Delta\theta$ was remarkable after contact both with RCA_{120} and with Con A. This result indicates that nonspecific adsorption of lectin occurred on these surfaces. In contrast, $\Delta\theta$ was only detected on PMBL when RCA_{120} was in contact with the surface; it increased with an increase in the fraction of the LAMA unit in PMBL. Although the absolute amount of RCA_{120} adsorbed on the PMBL1.0 surface was much lower than that adsorbed on the PBL1.0 surface, nonspecific adsorption of Con A was completely reduced on the PMBL1.0 surface.

On the PMB surface, the resonance angle was minimally changed. The behavior of protein adsorption resistance on MPC polymer surfaces has been reported in past literature.[29] The phosphorylcholine group of MPC polymers is very hydrophilic, which means that hydrophobic interaction with proteins is unlikely. Moreover, phosphorylcholine polymers minimally interact with the water structure around the polymer.[41] This is a unique property of phosphorylcholine polymers in comparison with the properties of conventional hydrophilic polymers. In addition, electrostatic interactions between a phosphorylcholine polymer surface and proteins are weak because the charge potential (ζ-potential) of phosphorylcholine is neutral.[42] Therefore, a phosphorylcholine polymer has several features that reduce nonspecific protein adsorption. Consequently, this polymer is one of the best polymer materials for forming nonbiofouling surfaces.

The XPS concentrations of oxygen and phosphorus of PMBL-coated surfaces were higher than the theoretical amount calculated from the bulk concentration, as is shown in Table 1. Thus, both functions of MPC and LAMA units represent preferable surface properties. A few mole percent of LAMA units incorporated into the copolymer did not influence the nonfouling properties of the MPC polymers and worked well as recognition sites for specific proteins.

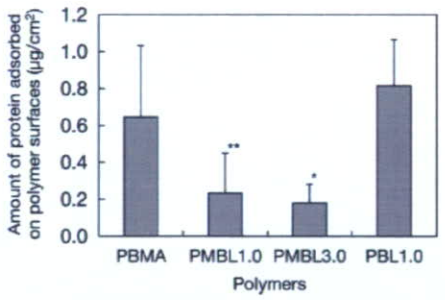

Figure 5. Amount of serum protein adsorbed on polymer surfaces after contact with cell culture medium for 60 min. $*p < 0.01$ PMBL3.0 vs PBMA and PMBL1.0 and $**p < 0.05$ PMBL1.0 vs PBL1.0.

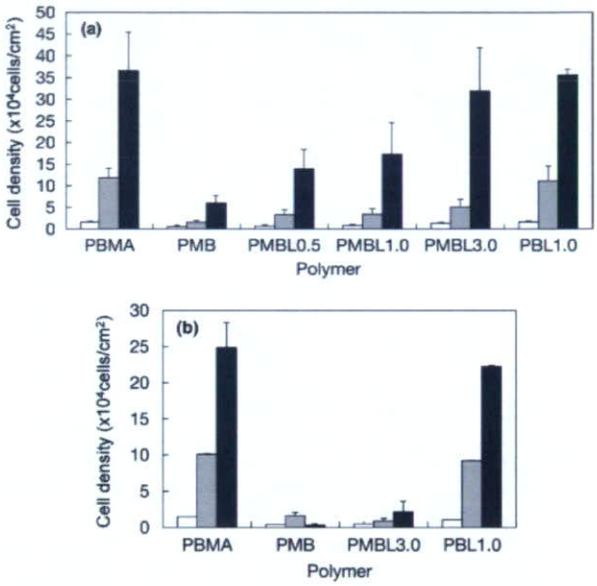

Figure 6. (a) Surface density on polymer surfaces after contact with HepG2 cells: (white) 24 h; (gray) 96 h; and (black) 168 h. (b) Surface density on polymer surfaces after contact with NIH/3T3 cells: (white) 24 h; (gray) 96 h; and (black) 168 h.

Cell Culture Experiment. The amount of adsorbed protein on the polymer surfaces is shown in Figure 5. The PMBL1.0 and -3.0 surfaces significantly reduced protein adsorption as compared to that on PBL1.0. The amount of protein adsorption on PMBL is similar to that on PMB, as previously described.[29] The amount of protein adsorption on PMBL is a level for the reduction of nonspecific cell adhesion.[27]

Figure 6a,b shows the time-dependent surface density of HepG2 and NIH-3T3 cells on a polymer surface after culturing for given periods, respectively. On a PBMA surface, many cells adhered, and the density increased with an increase in culture time. In contrast, cell adhesion was reduced on the PMB surface because adsorption of the cell adhesive protein on the surface could be reduced. Because the HepG2 cells have ASGPRs, which are galactose-recognizing receptors, cell adhesion was induced on the phosphorylcholine polymer surface having LAMA units. The cell density increased with an increase in the composition of LAMA units in the copolymers. When the LAMA composition was 3%, the density was similar to that on PBMA for every culture period (Figure 6a, PMBL3.0: $*p > 0.05$ vs PBMA and PBL1.0 and $**p < 0.01$ vs PMB).

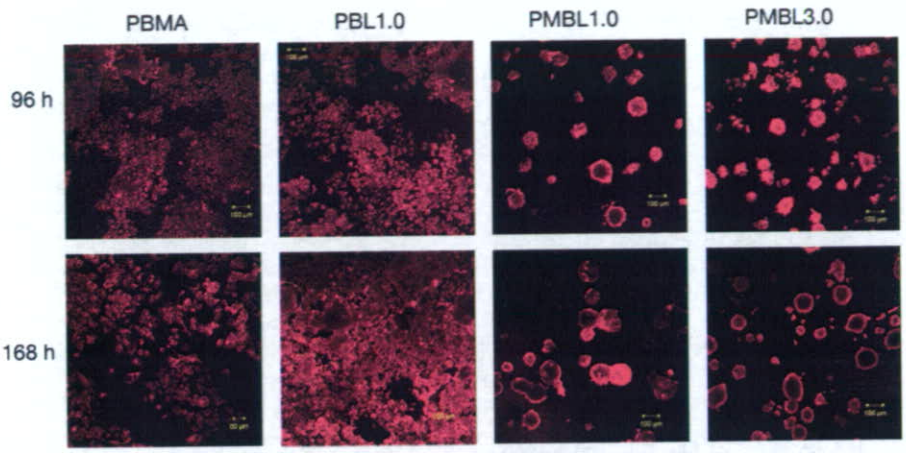

Figure 7. Fluorescence micrographs of polymer surfaces in contact with HepG2 cells for 96 and 168 h.

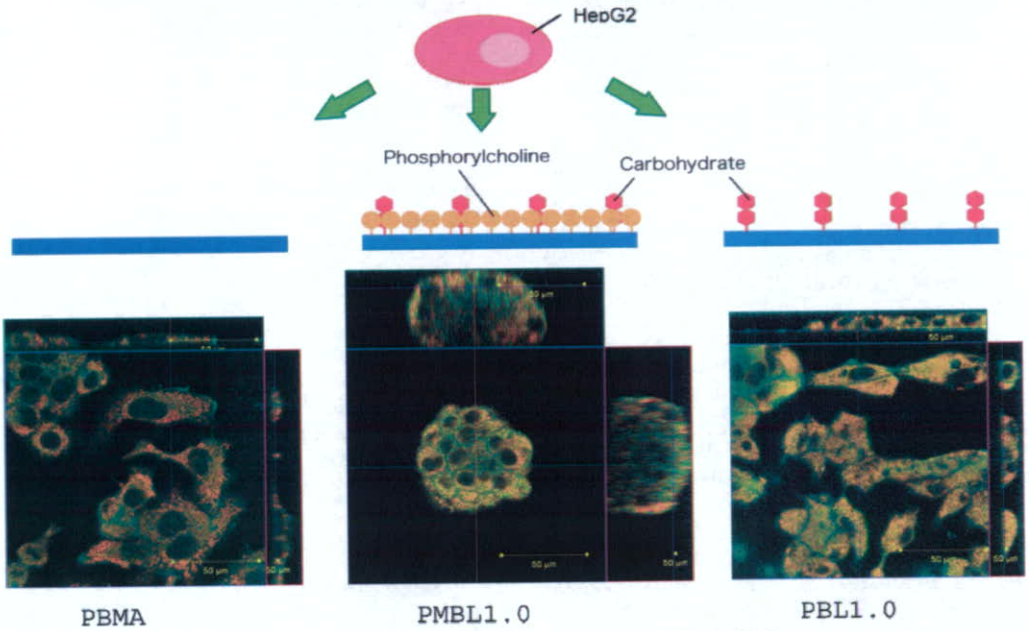

Figure 8. Confocal micrographs of adherent cells: (Green) F-actin and (red) phospholipid double layer.

NIH-3T3 cells do not have ASGPRs. On the PBMA surface, NIH-3T3 cells adhered and proliferated as well as the HepG2 cells did because much cell adhesive protein was adsorbed on the PBMA.[27] The LAMA unit in PBL did not affect NIH-3T3 cell adhesion, and a large number of NIH-3T3 cells adhered to the PBL1.0 surface. Because the PBL1.0 surface has a large amount of adsorbed protein containing cell adhesive protein such as fibronectin, integrin-mediated adhesion of NIH-3T3 cells on the PBL1.0 surface must have occurred. In contrast, the adhesion of NIH-3T3 cells was reduced on the polymer surfaces having MPC units (Figure 6b, PMBL3.0: $*p < 0.01$ vs PBMA and PBL1.0 and $**p > 0.05$ vs PMB). This result indicates that the ligand−receptor interaction at the polymer−cell interface worked preferably on the MPC polymers.

Spheroid Formation of HepG2 Cells. Figure 7 shows fluorescence micrographs of HepG2 cells cultured on polymer surfaces for 96 and 168 h. The membrane of the adherent cells was stained by Texas Red-DHPE. The adherent HepG2 cells on the PMBA surface were spread, and the morphology of each cell was easily observed. The HepG2 cells were also spread on the PBL1.0 surface, but some aggregation was observed. In contrast, the HepG2 cells observed on the PMBL1.0 and PMBL3.0 surfaces formed spheroids. The number of spheroids on PMBL increased with an increase in the number of LAMA units in the copolymer. The average diameter of the spheroids under each condition was calculated by measuring 50 random samples. Each amount was found to be as follows: 86.1 ± 26.7 μm (PMBL1.0, 96 h), 92.0 ± 28.9 μm (PMBL3.0, 96 h), 115.7 ± 28.6 μm (PMBL1.0, 168 h), and 125.8 ± 29.1 μm (PMBL3.0, 168 h). The number of cells forming a spheroid was calculated from the data shown in Figures 6a and 7 and was around 25 cells for the 96 h culture and 125 cells (PMBL1.0) and 160 cells (PMBL3.0) for the 168 h culture. The size of the spheroids increased with an increase in the number of LAMA units, indicating that the units play a role in holding the spheroids to the polymer surface.

For spheroid formation, a round-bottomed plate with a nonbinding surface was generally used. Although the process was very successful, only one large spheroid per well was obtained, and nutrition did not reach inside the cells of a spheroid, resulting in necrosis. In addition to the process of using round-bottomed wells with a nonbinding surface, spheroid formation of hepatocytes has been studied on polymer surfaces controlled chemically and/or physically. Akaike and co-workers

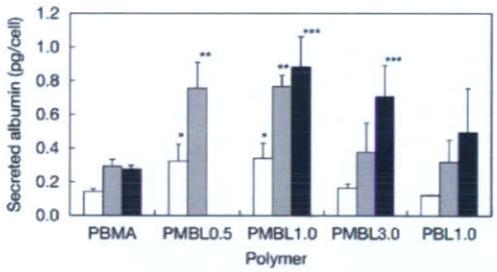

Figure 9. Amount of albumin secreted from adherent cells for 24 h after culturing of HepG2 cells on polymer surfaces for 96 (white), 168 (gray), and 360 h (black). $*p < 0.05$ vs PBMA in 96 h culture; $**p < 0.01$ vs PBMA in 168 h culture; and $***p < 0.01$ vs PBMA in 360 h culture.

are leading this field with the use of poly(*p*-*N*-vinylbenzyl-D-lactonamido) (PVLA). They reported that spheroid formation of hepatocytes on a PVLA surface could be observed with the addition of an epidermal growth factor (EGF).[43] The spheroid formation was also influenced by the morphologies of polymer surfaces such as honeycomb[44] and nanofibril[45] structures. On a PMBL surface, spheroid formation was induced on a flat surface and without the need for any growth factor or cytokine.

Figure 8 shows confocal micrographs of HepG2 cells cultured on PBMA, PBL1.0, and PMBL1.0 for 168 h. On PBMA and PBL1.0 surfaces, monolayer cell adhesion was observed, and each cell was spread. At the outline of the pseudo-pod formation of the adherent cells, actin was easily observed. In contrast, HepG2 cells cultured on PMBL1.0 formed spheroids with multilayer adhesion.

The mechanism of spheroid formation induced on PMBL surfaces is considered a nonintegrin-mediated adhesion phenomenon. The PMBL surfaces effectively reduce protein adsorption; the number of integrin binding sites on the surface is fewer than that on PBMA or PBL1.0 surfaces.

Albumin Secretion from Adherent HepG2. The functioning of HepG2 cells cultured on polymer surfaces was compared by measuring the amount of albumin secreted by the cells. Figure 9 shows the amount of albumin secreted by HepG2 cells for 24 h after 96 h (4 days), 168 h (7 days), and 360 h (15 days) of culturing on the polymer surfaces as determined by ELISA. At up to 168 h of culturing, the amount of albumin secreted per cell that adhered onto PMBL0.5 and -1.0 was significantly higher ($*p < 0.05$, 96 h and $**p < 0.01$, 168 h) than that on PBMA and PBL1.0. After culturing for 360 h, high amounts of albumin secreted from cells that adhered onto PMBL1.0 and -3.0 were observed ($***p < 0.01$). On PMBL0.5, reproducible data for 360 h of culturing were not obtained because the spheroids were easily detached from the surface. The density of the LAMA unit on the PMBL1.0 surface appeared to be optimal for preserving the ability to secrete albumin. Lu et al. recently reported that the functional maintenance of hepatocytes was enhanced with NIH/3T3 fibroblasts.[46] Although the mechanism has not been explained in detail, cell contact with NIH/3T3 cells constitutes a better condition for hepatocytes. PMBL has phosphorylcholine groups similar to the cell surface, and the surface may present a more suitable situation for hepatocyte growth as compared to that of PBMA or PBL.

There has been great interest in the potential utility of a bioartificial liver (BAL) device as a bridge support for patients who have suffered massive liver injury during the period until the regeneration of their own hepatocytes or until liver transplantation. Although preservation of cell function in the material surface is very important for this application, conventional polymer materials such as polysulfone, polyolefine, and polyurethane have generally been used.[47,48] Surface modification is important in further improving the function of BAL devices. We have reported that MPC polymers could be applied in the surface modification of hollow fibers that have the possibility of producing hemodialyzer and liver assist bioreactor devices.[49,50] We have applied PMBL as a coating material for polypropylene hollow fiber mini-modules, which are the subject of a long-term cell culture study. PMBL can reduce nonspecific biofouling, thus efficiently preserving the mass transport ability of hollow fiber membranes. In addition, the polymer can provide a more suitable environment for cell cultivation than that of conventional hollow fiber materials.

Conclusion

Carbohydrate-immobilized phosphorylcholine polymers (PMBL) were newly synthesized to produce biomembrane mimetic surfaces, which perform selective recognition of proteins and cells. Surfaces coated with PMBL effectively reduced nonspecific interactions, and a specific ligand−receptor interaction was clearly demonstrated. In this study, we used HepG2 cells to recognize galactose. The morphology of the cells and their functions on a PMBL surface were significantly different from those on a PBMA surface. LAMA units and MPC units of PMBL are important for supporting hepatocytes and for reducing nonspecific interactions at the cell−material interface, respectively. Yin et al. compared the morphology of cancer cells and primary cells on galactose-immobilized substrates.[51] They stated that no significant difference in spheroid formation based on these cells was observed. Therefore, the primary hepatic cell might form spheroids on the PMBL surface. The primary cell function on the PMBL surface will be reported in the near future.

We clarified that carbohydrates immobilized on the phosphorylcholine polymer surface were easily distinguished from the specific protein and cells. Changing the types of carbohydrates enables changes in the types of biorecognition. The polymers have great potential for bioreaction, molecular separation, targeting, sensing, etc.

Acknowledgment. We thank the New Energy and Industrial Technology Development Organization (NEDO) Japan (Industrial Technology Research Grant in 2004, 04A02025) for providing financial support.

References and Notes

(1) Ratner, B. D. The engineering of biomaterials exhibiting recognition and specificity. *J. Mol. Recognit.* **1996**, *9*, 617−625.
(2) Ratner, B. D. New ideas in biomaterials science−A path to engineered biomaterials. *J. Biomed. Mater. Res.* **1993**, *27*, 837−850.
(3) Lee, J. H.; Lee, H. B. A wettability gradient as a tool to study protein adsorption and cell adhesion on polymer surfaces. *J. Biomater. Sci., Polym. Ed.* **1993**, *4*, 467−481.
(4) Mrksich, M.; Chen, C. S.; Xia, Y.; Dike, L. E.; Ingber, D. E.; Whitesides, G. M. Controlling cell attachment on contoured surfaces with self-assembled monolayers of alkanethiolates on gold. *Proc. Natl. Acad. Sci. U.S.A.* **1996**, *93*, 10775−10778.
(5) Ito, Y. Surface micropatterning to regulate cell functions. *Biomaterials* **1999**, *20*, 2333−2342.
(6) Massia, S. P.; Hubbell, J. A. Human endothelial cell interactions with surface-coupled adhesion peptides on a nonadhesive glass substrate and two polymeric biomaterials. *J. Biomed. Mater. Res.* **1991**, *25*, 223−242.
(7) Lin, H. B.; Garcia-Echeverria, C.; Asakura, S.; Sun, W.; Mosher, D. F.; Cooper, S. L. Endothelial cell adhesion on polyurethanes containing covalently attached RGD peptides. *Biomaterials* **1992**, *13*, 905−914.
(8) Sugawara, T.; Matsuda, T. Photochemical surface derivatization of a peptide containing Arg−Gly−Asp (RGD). *J. Biomed. Mater. Res.* **1995**, *29*, 1047−1052.

(9) Shakesheff, K.; Cannizzaro, S.; Langer, R. Creating biomimetic microenvironments with synthetic polymer−peptide hybrid molecules. *J. Biomater. Sci., Polym. Ed.* **1998**, *9*, 507−518.
(10) VandeVondele, S.; Voros, J.; Hubbell, J. A. RGD-grafted poly-L-lysine-graft-(poly(ethylene glycol)) copolymers block non-specific protein adsorption while promoting cell adhesion. *Biotechnol. Bioeng.* **2003**, *82*, 784−790.
(11) Murphy, W. L.; Mercurius, K. O.; Koide, S.; Mrksich, M. Substrates for cell adhesion prepared via active site-directed immobilization of a protein domain. *Langmuir* **2004**, *20*, 1026−1030.
(12) Hersel, U.; Dahmen, C.; Kessler, H. RGD modified polymers: Biomaterials for stimulated cell adhesion and beyond. *Biomaterials* **2003**, *24*, 4385−4415.
(13) Massia, S. P.; Hubbell, J. A. An RGD spacing of 440 nm is sufficient for integrin α V β 3-mediated fibroblast spreading and 140 nm for focal contact and stress fiber formation. *J. Cell Biol.* **1991**, *114*, 1089−1100.
(14) Kobayashi, A.; Kobayashi, K.; Akaike, T. Control of adhesion and detachment of parenchymal liver cells using lactose-carrying polystyrene as substratum. *J. Biomater. Sci., Polym. Ed.* **1992**, *3*, 499−508.
(15) Gestwicki, J. E.; Cairo, C. W.; Mann, D. A.; Owen, R. M.; Kiessling, L. L. Selective immobilization of multivalent ligands for surface plasmon resonance and fluorescence microscopy. *Anal. Biochem.* **2002**, *305*, 149−155.
(16) Pricer, W. E.; Hudgin, R. L.; Ashwell, G.; Stockert, R. J.; Morell, A. G. A membrane receptor protein for asialoglycoproteins. *Methods Enzymol.* **1974**, *34*, 688−691.
(17) Stockert, R. J. The asialoglycoprotein receptor: Relationships between structure, function, and expression. *Physiol. Rev.* **1995**, *75*, 591−609.
(18) Weigel, P. H.; Scnnaar, R. L.; Kuhlenschmidt, M. S.; Schmell, E.; Lee, R. T.; Lee, Y. C.; Roseman, S. Adhesion of hepatocytes to immobilized sugars. A threshold phenomenon. *J. Biol. Chem.* **1979**, *254*, 10830−10838.
(19) Kobayashi, A.; Akaike, T.; Kobayashi, K.; Sumitomo, H. Enhanced adhesion and survival efficacy of liver cells in culture dishes coated with a lactose-carrying styrene homopolymer. *Makromol. Chem., Rapid Commun.* **1986**, *7*, 645−650.
(20) Gutsche, A. T.; Parsons-Wingerter, P.; Chand, D.; Saltzman, W. M.; Leong, K. W. *N*-Acetylglucosamine and adenosine derivatized surfaces for cell culture, 3T3 fibroblast, and chicken hepatocyte response. *Biotechnol. Bioeng.* **1994**, *43*, 801−809.
(21) Sagara, K.; Kim, S. W. A new synthesis of galactose-poly(ethylene glycol)-polyethylenimine for gene delivery to hepatocytes. *J. Controlled Release* **2002**, *79*, 271−281.
(22) Kim, S. H.; Hoshiba, T.; Akaike, T. Hepatocyte behavior on synthetic glycopolymer matrix: Inhibitory effect of receptor−ligand binding on hepatocyte spreading. *Biomaterials* **2004**, *25*, 1813−1823.
(23) Sato, K.; Miura, Y.; Saito, N.; Kobayashi, K.; Takai, O. *Biomacromolecules* **2007**, *8*, 753−756.
(24) Yarema, K. J.; Mahal, L. K.; Bruehl, R. E.; Rodriguez, E. C.; Bertozzi, C. R. Metabolic delivery of ketone groups to sialic acid residues. Application to cell surface glycoform engineering. *J. Biol. Chem.* **1998**, *273*, 31168−31179.
(25) Iwasaki, Y.; Mikami, A.; Kurita, K.; Yui, N.; Ishihara, K.; Nakabayashi, N. Reduction of surface-induced platelet activation on phospholipid polymers. *J. Biomed. Mater. Res.* **1997**, *36*, 508−515.
(26) Iwasaki, Y.; Sawada, S.; Nakabayashi, N.; Khang, G.; Lee, H. B.; Ishihara, K. The effect of the chemical structure of the phospholipid polymer on fibronectin adsorption and fibroblast adhesion on the gradient phospholipid surface. *Biomaterials* **1999**, *20*, 2185−2191.
(27) Ishihara, K.; Ishikawa, E.; Iwasaki, Y.; Nakabayashi, N. Inhibition of fibroblast cell adhesion on substrate by coating with 2-methacryloyloxyethyl phosphorylcholine polymers. *J. Biomater. Sci., Polym. Ed.* **1999**, *10*, 1047−1061.
(28) Iwasaki, Y.; Nakabayashi, N.; Ishihara, K. Preservation of platelet function on 2-methacryloyloxyethyl phosphorylcholine-graft polymer as compared to various water-soluble graft polymers. *J. Biomed. Mater. Res.* **2001**, *57*, 72−78.
(29) Ishihara, K.; Oshida, H.; Endo, Y.; Ueda, T.; Watanabe, A.; Nakabayashi, N. Hemocompatibility of human whole blood on polymers with a phospholipid polar group and its mechanism. *J. Biomed. Mater. Res.* **1992**, *26*, 1543−1552.
(30) Ishihara, K.; Nomura, H.; Mihara, T.; Kurita, K.; Iwasaki, Y.; Nakabayashi, N. Why do phospholipid polymers reduce protein adsorption? *J. Biomed. Mater. Res.* **1998**, *39*, 323−330.
(31) Iwasaki, Y.; Sawada, S.; Ishihara, K.; Khang, G.; Lee, H. B. Reduction of surface-induced inflammatory reaction on PLGA/MPC polymer blend. *Biomaterials* **2002**, *23*, 3897−3903.
(32) Sawada, S.; Sakaki, S.; Iwasaki, Y.; Nakabayashi, N.; Ishihara, K. Suppression of the inflammatory response from adherent cells on phospholipid polymers. *J. Biomed. Mater. Res.* **2003**, *64*, 411−416.
(33) Ishihara, K.; Ueda, T.; Nakabayashi, N. Preparation of phospholipid polymers and their properties as polymer hydrogel membranes. *Polym. J.* **1990**, *22*, 355−360.
(34) Narain, R.; Armes, S. P. Synthesis and aqueous solution properties of novel sugar methacrylate-based homopolymers and block copolymers. *Biomacromolecules* **2003**, *4*, 1746−1758.
(35) Matsuura, K.; Kobayashi, K. Analysis of GM3−Gg3 interaction using clustered glycoconjugate models constructed from glycolipid monolayers and artificial glycoconjugate polymers. *Glycoconjugate J.* **2004**, *21*, 139−148.
(36) Iwasaki, Y.; Fujiike, A.; Kurita, K.; Ishihara, K.; Nakabayashi, N. Protein adsorption and platelet adhesion on polymer surfaces having a phospholipid polar group connected with oxyethylene chain. *J. Biomater. Sci., Polym. Ed.* **1996**, *8*, 91−102.
(37) Tsai, W. B.; Grunkemeier, J. M.; Horbett, T. A. Human plasma fibrinogen adsorption and platelet adhesion to polystyrene. *J. Biomed. Mater. Res.* **1999**, *44*, 130−139.
(38) Haslam, G.; Wyatt, D.; Kitos, P. A. Estimating the number of viable animal cells in multi-well cultures based on their lactate dehydrogenase activities. *Cytotechnology* **2000**, *32*, 63−75.
(39) Lee, Y. C. Biochemistry of carbohydrate−protein interaction. *FASEB J.* **1992**, *26*, 3193−3200.
(40) Matsuura, K.; Hayashi, K.; Kobayashi, K. On-off switching of gene expression regulated with carbohydrate-lectin interaction. *Biomacromolecules* **2005**, *6*, 2533−2540.
(41) Ishihara, K.; Nomura, H.; Mihara, T.; Kurita, K.; Iwasaki, Y.; Nakabayashi, N. Why do phospholipid polymers reduce protein adsorption? *J. Biomed. Mater. Res.* **1998**, *39*, 323−330.
(42) Ishihara, K.; Inoue, H.; Kurita, K.; Nakabayashi, N. Selective adhesion of platelets on a polyion complex composed of phospholipid polymers containing sulfonate groups and quarternary ammonium groups. *J. Biomed. Mater. Res.* **1994**, *28*, 1347−1355.
(43) Tobe, S.; Takei, Y.; Kobayashi, K.; Akaike, T. Receptor-mediated formation of multilayer aggregates of primary cultured adult rat hepatocytes on lactose-substituted polystyrene. *Biochem. Biophys. Res. Commun.* **1992**, *184*, 225−230.
(44) Tanaka, M.; Nishikawa, K.; Okubo, H.; Kamachi, H.; Kawai, T.; Matsushita, M.; Todo, S.; Shimomura, M. Control of hepatocyte adhesion and function on self-organized honeycomb-patterned polymer film. *Colloids Surf., A* **2006**, *284*, 464−469.
(45) Chua, K. N.; Lim, W. S.; Zhang, P.; Lu, H.; Wen, J.; Ramakrishna, S.; Leong, K. W.; Mao, H. Q. Stable immobilization of rat hepatocyte spheroids on galactosylated nanofiber scaffold. *Biomaterials* **2005**, *26*, 2537−2547.
(46) Lu, H. F.; Chua, K. N.; Zhang, P. C.; Lim, W. S.; Ramakrishna, S.; Leong, K. W.; Mao, H. Q. Three-dimensional co-culture of rat hepatocyte spheroids and NIH/3T3 fibroblasts enhances hepatocyte functional maintenance. *Acta Biomater.* **2005**, *1*, 399−410.
(47) Mizumoto, H.; Funatsu, K. Liver regeneration using a hybrid artificial liver support system. *Artif. Organs* **2004**, *28*, 53−57.
(48) Long, L.; Liu, Z.; Wang, T.; Deng, X.; Yang, K.; Li, L.; Zhao, C. Polyethersulfone dead-end tube as a scaffold for artificial lacrimal glands in vitro. *J. Biomed. Mater. Res., Part B* **2006**, *78*, 409−416.
(49) Hasegawa, T.; Iwasaki, Y.; Ishihara, K. Preparation of blood-compatible hollow fibers from a polymer alloy composed of polysulfone and 2-methacryloyloxyethyl phosphorylcholine polymer. *J. Biomed. Mater. Res.* **2002**, *63*, 333−341.
(50) Ye, S. H.; Watanabe, J.; Takai, M.; Iwasaki, Y.; Ishihara, K. Design of functional hollow fiber membranes modified with phospholipid polymers for application in total hemopurification systems. *Biomaterials* **2005**, *26*, 5032−5041.
(51) Yin, C.; Liao, K.; Mao, H. Q.; Leong, K. W.; Zhuo, R. X.; Chan, V. Adhesion contact dynamics of HepG2 cells on galactose-immobilized substrates. *Biomaterials* **2003**, *24*, 837−850.

BM700478D

Control of cell function on carbohydrate-immobilized phosphorylcholine polymer surfaces

Y.Iwasaki[1], U.Takami[2], Y.Shinohara[2], K.Akiyoshi[2]

[1] *Kansai University, Osaka, Japan.* [2] *Tokyo Medical and Dental University, Tokyo, Japan.*

INTRODUCTION: We hypothesized that 2-methacryloyloxyethyl phosphorylcholine (MPC) polymer surfaces bearing carbohydrates might perform as biomembrane mimetic surfaces, which can interact with a specific cell. In this study, MPC copolymers with galactose residues have been synthesized and we present here the effectiveness of the surface in controlling cell/material interaction and preserving cell function.

METHODS: Poly[MPC-co-n-butyl methacrylate (BMA)] (PMB), poly[BMA-co-2-lactobionamidoethyl methacrylate (LAMA)] (PBL), and poly(MPC-co-BMA-co-LAMA) (PMBL) were synthesized by conventional radical polymerization[1].

Human hepatocellular liver carcinoma cell line (HepG2) cells and mouse fibroblasts (NIH-3T3) were purchased from RIKEN Cell Bank. The concentration of the cells was adjusted to 2.0×10^4 cells/ml. The cells were seeded on the polymer surfaces and continuously cultured for specific periods. The polymer plates were then rinsed with PBS. The plates were soaked into Triton X-100 aqueous solution. The Triton X-100 solution was collected and the concentration of LDH from the adherent cells was measured.

Morphological observation of the HepG2 cells cultured on the polymer surfaces was performed by a confocal laser scanning microscope.

RESULTS: Figure 1 shows the time-dependent surface density of HepG2 and NIH-3T3 cells on a polymer surface after culture for given periods. On a PBMA surface, many HepG2 cells adhered and the density increased with an increase in culture time. In contrast, the cell adhesion was reduced on the PMB surface because adsorption of the cell-adhesive protein on the surface could be reduced (data not shown). When the LAMA composition was 3% in PMBL, the density of adherent HepG2 cells was similar to that on PBMA for every culture period. NIH-3T3 cells adhered and proliferated as well as the HepG2 cells on the PBMA surface. On the other hand, the adhesion of NIH-3T3 cells was reduced on the polymer surfaces having MPC units.

Figure 2 shows confocal micrographs of HepG2 cells cultured on PBMA, PBL1.0, and PMBL1.0 for 168 h. On PBMA and PBL1.0 surfaces, monolayer cell adhesion was observed and each cell was spread. At the outline of the pseudopod formation of the adherent cells, actin was easily observed. In contrast, HepG2 cells cultured on PMBL1.0 formed spheroids with multilayer adhesion.

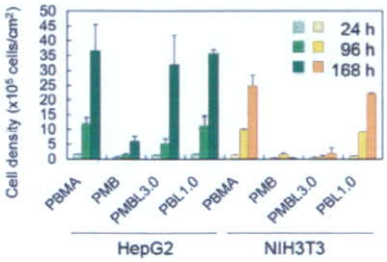

Fig. 1: Cell density on polymer surfaces.

DISCUSSION & CONCLUSIONS: Carbohydrate-immobilized phosphorylcholine polymers (PMBL) were newly synthesized to produce biomembrane mimetic surfaces, which perform selective recognition of proteins and cells. Surfaces coated with PMBL effectively reduced nonspecific interaction, and specific ligand/receptor interaction was clearly demonstrated. Changing the types of carbohydrates enables changes in the types of biorecognition. The polymers have great potential for bioreaction, molecular separation, targeting, sensing, etc.

REFERENCES: [1] Y. Iwasaki, U.Takami. Y.Shinohara, et al (2007) *Biomacromolecules*, in press.

ACKNOWLEDGEMENTS: We thank the New Energy and Industrial Technology Development Organization (NEDO) Japan for providing financial support.

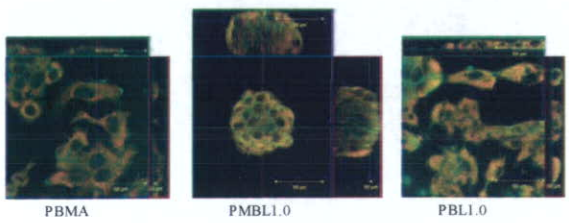

Fig. 2: Fluorescence micrographs of adherent cells.

European Cells and Materials Vol. 14. Suppl. 3, 2007 (page 66) ISSN 1473-2262

Site-directed immobilization of antibodies on well-defined polymer brushes

R.Iwata[1], Y.Iwasaki[2], K.Akiyoshi[1]

[1] *Institute of Biomaterials and Bioengineering, Tokyo Medical and Dental University, Tokyo, Japan.*
[2] *Faculty of Chemistry, Materials and Bioengineering, Kansai University, Osaka, Japan.*

INTRODUCTION: Surface characteristics for biosensor applications require both reducing non-specific biofouling and enhancing specific recognition. Especially in the protein-chip technology, immobilization of proteins in proper orientation is necessary to maintain the biological activities. We have reported that 2-methacryloyloxyethyl phosphorylcholine (MPC) polymers synthesized as biomimetics in biomembrane structures significantly reduce protein adsorption and cell adhesion[1]. Furthermore, manipulation of protein and cell was well performed on well-defined poly(MPC) (PMPC) brushes produced by atom transfer radical polymerization (ATRP)[2]. The block copolymer brushes consisting of PMPC and poly[glycidyl methacrylate (GMA)] were also recently prepared for engineered biomaterial surfaces[3]. We describe here about oriented immobilization of antibodies onto the polymer brushes for biorecognition surfaces.

METHODS: Polymer brushes consisting of PMPC and poly(GMA) (PGMA) were formed on silicon wafers by ATRP as described previously[3]. Pyridyl disulfide moieties were then introduced to the polymer brushes via epoxy groups in GMA unit. Fab' fragments (Goat anti-mouse IgG) solution was in contact with polymer brushes with pyridyl disulfide moieties and reacted at room temperature over night. After the immobilization of Fab' fragments and wash with buffer, 1% bovine serum albumin (BSA) was applied to surfaces and incubated for 1h at room temperature. Fluorescein isothiocyanate- (FITC-) labeled immunoglobulin (Mouse anti-rat IgG) was used as antigen. BSA solution was removed and antigen solution was in contact with polymer brushes with Fab' fragments for 1 h at room temperature. After wash and dried, the fluorescence intensity was analyzed.

RESULTS: Fab' fragment is one of the antibody fragments and has thiol group in the opposite side of antigen-binding domain. We can immobilize the Fab' fragments in ordered orientation via thiol-disulfide exchange between the thiol groups of Fab' fragments and pyridyl disulfide moieties in polymer brushes. To compare the amount of immobilized antibody, FITC-labeled Fab' fragments were reacted with each surfaces and the fluorescence intensity was determined. We prepared the organosilane monolayer having epoxy groups (epoxysilane films) as a control surface. The amount of immobilized antibody increased with an increase in the length of GMA unit. PGMA brush immobilized largest amount of antibody. Fig. 1 shows the ratio of fluorescence intensity of each surface after contact with FITC-labeled antigen. The fluorescence intensity of polymer brushes was higher than that of epoxysilane. In PMPC-*b*-PGMA brushes, the fluorescence intensity increased with an increase in the thickness of PGMA.

DISCUSSION & CONCLUSIONS: The amount of immobilized Fab' fragments and subsequent reaction with antigen could be controlled by changing the thickness of polymer brushes. Although PGMA brush surface has larger amount of Fab' fragment compared with PMPC-*b*-PGMA brush with longer PGMA, the reactivity with antigen was similar on these surfaces (Fig. 1.). It is considered that the condition of immobilized Fab' fragments are different between PGMA brush and PMPC-*b*-PGMA brush which has biocompatible PMPC under PGMA. It was also shown that polymer brush surface for reaction with antigen was more effective than the epoxysilane films. The characteristics of PMPC and dense immobilization of antibodies in defined orientation are effective in high sensitive biorecognition.

REFERENCES: [1]S. Sawada, S. Sakaki, Y. Iwasaki, N. Nakabayashi, K. Ishihara (2003) *J Biomed Mater Res* **64A**:411-416. [2]R. Iwata, P. Suk-In, V.P. Hoven, A. Takahara, K. Akiyoshi, Y. Iwasaki (2004) *Biomacromolecules* **5**:2308-2314. [3]R. Iwata, Y. Iwasaki, K. Akiyoshi, A. Takahara (2005) *Trans. Mater. Res. Soc. Jpn* **30**:735-738.

ACKNOWLEDGEMENTS: The authors of this paper would like to thank Japan Society for the Promotion of Science for financial support of this research.

Novel Thermoresponsive Polymers Having Biodegradable Phosphoester Backbones

Yasuhiko Iwasaki,*,† Chookaet Wachiralarpphaithoon,‡ and Kazunari Akiyoshi‡,§

Department of Chemistry and Materials Engineering, Faculty of Chemistry, Materials and Bioengineering, Kansai University, 3-3-35 Yamate-cho, Suita-shi, Osaka 564-8680, Japan, Institute of Biomaterials and Bioengineering, Tokyo Medical and Dental University, 2-3-10 Kanda-surugadai, Chiyoda-ku, Tokyo 101-0062, Japan, and Center of Excellence Program for Frontier Research on Molecular Destruction and Reconstruction of Tooth and Bone, Tokyo Medical and Dental University, 2-3-10 Kanda-surugadai, Chiyoda-ku, Tokyo 101-0062, Japan

Received July 13, 2007
Revised Manuscript Received September 24, 2007

Introduction. Thermoresponsive polymers are widely studied in both research and technology because of their versatility in many fields. Recent trends in polymer materials are drug delivery,[1] separation of bioactive molecules,[2] and tissue engineering.[3] N-substituted acrylamide polymers have been found to have a phase separation characteristic with changes occurring in their properties upon heating above a certain lower critical solution temperature (LCST).[4−6] In particular *N*-isopropylacrylamide (NIPAAm) is one of the best monomers for accomplishing this and the homopolymer has LCST at 32 °C in aqueous solution.[7] NIPAAm can be applied to polymerization with a wide variety of comonomers and the LCST of the polymers can be controlled around physiological temperatures.[8,9] Furthermore, living radical polymerization has recently been applied with NIPAAm for the preparation of smart polymers with well-defined structures.[10−12] Although NIPAAm is a robust monomer for obtaining thermoresponsive polymer materials such as stimuli-responsive surfaces, particles, and hydrogels, the polymers are not biodegradable.

As well as a stimuli-responsive nature, biodegradability and biocompatibility are important characteristics for polymeric materials used in biomedical fields. While the thermoresponsivity of some biodegradable polymers such as aliphatic polyester block copolymers or polypeptides was recently proposed,[13−16] the molecular design and synthetic process of thermoresponsive biodegradable polymers are still limited. N-substituted acrylamide polymers are thus preferably studied.

Recently, polyphosphoesters have appeared interesting for biological and pharmaceutical applications because of their biocompatibility and structural similarities to naturally occurring nucleic and teichoic acids. Polyphosphoesters have been proposed for use in the field of biomaterials.[17−20] A variety of synthetic routes for polyphosphoesters has been proposed including ring-opening polymerization,[21,22] polycondensation,[23] transesterfication,[24,25] and enzymatic polymerization.[26] There has been a great deal of interest in polyphosphoesters, which are biodegradable through hydrolysis and possibly through enzymatic digestion of phosphate linkages under physiological conditions.[27] Although polyphosphoesters are very interesting polymers, there is no report of any thermoresponsive properties. In current research, thermoresponsive polyphosphoesters are being newly synthesized with simple copolymerization of cyclic phosphoester compounds and their properties are being investigated.

Results and Discussion. 2-Ethoxy-2-oxo-1,3,2-dioxaphospholane (EP) and 2-isopropoxy-2-oxo-1,3,2-dioxaphospholane (IPP) were synthesized by the previously described method.[28] Poly(IPP-*co*-EP) (PI_xE_yP; x = IPP (mol %); y = EP (mol %)) was synthesized by ring-opening polymerization using triisobutyl aluminum (iBu$_3$Al) as an initiator (Scheme 1). The polymerization was homogeneously performed by a solvent-free reaction. The polymers were dissolved in ethanol and purified by reprecipitation into diethyl ether. The range of weight-averaged molecular weights was 1.2×10^4 to 1.5×10^4 g/mol by gel-permeation chromatography through a Polymer Laboratories MIXED-C column using a calibration curve based on linear polystyrene standards and their molecular weight distribution was lower than 1.3. Chloroform was the GPC solvent. The molar fraction of IPP and EP in the copolymer was calculated from a ^{1}H NMR spectrum. ^{1}H NMR (270 MHz, $CDCl_3$): δ = PI_xE_yP: 1.21−1.47 (m; $-CH_3$, 6H in IPP and 3H in EP), 3.95−4.20 (m; $-CH_2-$, 2H in EP and $-OCH_2CH_2O-$, 4H in backbone), 4.58 (m; $-CH(CH_3)_2$ in IPP, 1H).

The polymerization ratio (r_1/r_2) of IPP and EP was 0.48/2.23 as determined by the Fineman-Ross method. The reactivity of EP was much higher than that of IPP. Chen and co-workers compared the polymerization ability of IPP and EP using stannous octoate as an initiator.[29] In their data, the higher reactivity of EP was also observed.

Figure 1 is a typical photograph of aqueous solutions of $PI_{24}E_{76}P$, which has 24-mol % IPP and 76-mol % EP. The solution was transparent at 20 °C, but it was turbid at 40 °C. The LCST of $PI_{24}E_{76}P$ was 31 °C, as determined from the middle point of the transition state of transmittance using JASCO software.

Figure 2 shows the effect of the composition of the monomer unit on the LCST of the copolymers. The LCST of poly(EP) (PEP) was 38 °C and it linearly decreased with an increase in the composition of IPP. IPP is relatively hydrophobic, the homopolymer of IPP is not soluble in water above 5 °C. Dehydration of the polymer then preferably occurred with the addition of the hydrophobic IPP unit. It is reported that the LCST of thermoresponsive polymers can be controlled by compositions of hydrophobic and hydrophilic units.[8,15] Thermoresponsivity under physiological conditions is effective for drug delivery or tissue engineering applications.[30,31] The thermoresponsivity of polyphosphoesters can also be observed under physiological temperatures. Thus, the polymers are applicable in biomedical field.

Figure 3 shows the repeated temperature dependence of the transmittance of light through a $PI_{24}E_{76}P$ aqueous solution. While the hysteresis of change in transmittance between the variations in temperature was observed, the curve coincided well with the variation regardless of the number of repetitions. The polymer associate then completely disintegrated at the low temperature. The hydrodynamic radii (R_h) of $PI_{24}E_{76}P$ in an

* Corresponding author. Fax: +81-6-6368-0090. Telephone: +81-6-6368-0090. E-mail: yasu.bmt@ipcku.kansai-u.ac.jp.
† Department of Chemistry and Materials Engineering, Faculty of Chemistry, Materials and Bioengineering, Kansai University.
‡ Institute of Biomaterials and Bioengineering, Tokyo Medical and Dental University.
§ Center of Excellence Program for Frontier Research on Molecular Destruction and Reconstruction of Tooth and Bone, Tokyo Medical and Dental University.

10.1021/ma0715573 CCC: $37.00
Published on Web 10/12/2007

Scheme 1. Synthetic Route of PI_xE_yP

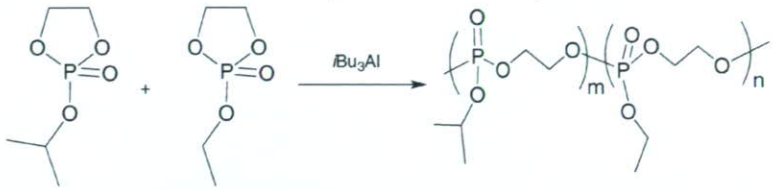

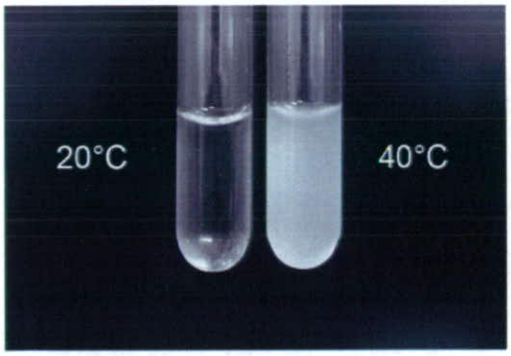

Figure 1. Photograph of $PI_{24}E_{76}P$ aqueous solution at 20 and 40 °C.

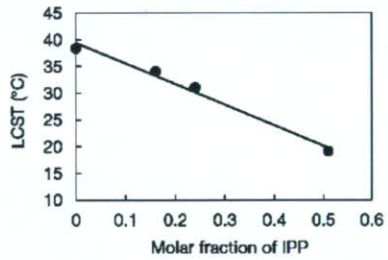

Figure 2. Effect of molar fraction of IPP on LCST of PI_xE_yP.

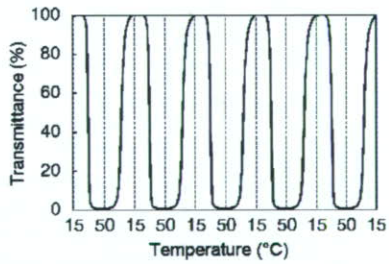

Figure 3. Change in the transmittance of polymer solution by repeated thermal cycling.

aqueous solution were also investigated using the Malvern dynamic light scattering technique. When the R_h of $PI_{24}E_{76}P$ at below 20 °C was 6.7 ± 0.1 nm, the polymer associate with more than 6 μm R_h was formed at 50 °C. The phase separation behavior of the polymer was easily reproducible.

Hydrogels[30,31] and nanoparticles[32,33] have been prepared using polyphosphoesters as macrocross-linkers and macroinitiators, respectively. In the former literatures, the enzymatic digestion and nonenzymatic degradation of polyphosphoesters were investigated. Typically, the rate of degradation of a hydrogel cross-linked with polyphosphoesters was increased with an increase in the concentration of alkaline phosphatase in the soaking medium. Furthermore, the cytotoxicity of the polyphosphoesters and the degradation products were not observed. These polyphosphoesters have been recently studied as artificial cellular matrices and nanoparticles for drug delivery systems.

The possibility of varied molecular designs and changeable solubility of polyphosphoesters can be looked upon as an advantage of the polymers in comparison with conventional biodegradable polymers such as aliphatic polyesters.

In conclusion, thermoresponsive polyphosphoesters were newly obtained from the copolymerization of two cyclic phosphoester monomer components. The LCST of the copolymers could be easily controlled with the composition and the thermoresponsivity of the polymers was ably reproducible. Thermoresponsive polyphosphoesters have great potential as novel smart biomaterials.

Acknowledgment. The authors acknowledge financial support from Mukai Science and Technology Foundation. The authors are grateful to Mr. Kazuaki Ikoma and Mr. Takashi Kawakita for their experimental support.

Supporting Information Available: Text giving experimental procedures and synthetic results of polymers, a table of synthetic results, and a figure showing the effect of temperature on light transmittance. This material is available free of charge via the Internet at http://pubs.acs.org.

References and Notes

(1) Kikuchi, A.; Okano, T. *Adv. Drug Deliv. Rev.* **2002**, *54*, 53−77.
(2) Kobayashi, J.; Kikuchi, A.; Sakai, K.; Okano, T. *Anal. Chem.* **2003**, *75*, 3244−3249.
(3) Kikuchi, A.; Okano, T. *J. Controlled Release* **2005**, *101*, 69−84.
(4) Monji, N.; Cole, C. A.; Hoffman, A. S. *J. Biomater. Sci., Polym. Ed.* **1994**, *5*, 407−420.
(5) Yamazaki, A.; Winnik, F. M.; Cornelius, R. M.; Brash, J. L. *Biochim. Biophys. Acta* **1999**, *1421*, 103−115.
(6) Idziak, I.; Avoce, D.; Lessard, D.; Gravel, D.; Zhu, X. X. *Macromolecules* **1999**, *32*, 1260−1263.
(7) Heskins, M.; Guillent, J. E.; James, E. *J. Macromol. Sci. Chem.* **1968**, *A2*, 1441−1445.
(8) Takei, Y. G.; Aoki, T.; Sanui, K.; Ogata, N.; Okano, T.; Sakurai, Y. *Bioconjug. Chem.* **1993**, *4*, 341−346.
(9) Feil, H.; Bae, Y. H.; Feijen, J.; Kim, S. W. *Macromolecules* **1993**, *26*, 2496−2500.
(10) Hales, M.; Barner-Kowollik, C.; Davis, T. P.; Stenzel, M. H. *Langmuir* **2004**, *20*, 10809−10817.
(11) Kulkarni, S.; Schilli, C.; Grin, B.; Muller, A. H. E.; Hoffman, A. S.; Stayton, P. S. *Biomacromolecules* **2006**, *7*, 2736−2741.
(12) Lokuge, I.; Wang, X.; Bohn, P. W. *Langmuir* **2007**, *23*, 305−311.
(13) Fujiwara, T.; Mukose, T.; Yamaoka, T.; Yamane, H.; Sakurai, S.; Kimura, Y. *Macromol. Biosci.* **2001**, *1*, 204−208.
(14) Kim, M. S.; Seo, K. S.; Khang, G.; Cho, S. H.; Lee, H. B. *J. Polym. Sci., Part A: Polym. Chem.* **2004**, *42*, 5784−5793.
(15) Tachibana, Y.; Kurisawa, M.; Uyama, H.; Kakuchi, T.; Kobayashi, S. *Chem. Commun.* **2003**, 106−107.
(16) Shimokuri, T.; Kaneko: T.; Akashi, M. *Macromol. Biosci.* **2006**, *6*, 942−951.
(17) Wan, A. C.; Mao, H. Q.; Wang, S.; Leong, K. W.; Ong, L. K.; Yu, H. *Biomaterials* **2001**, *22*, 1157−1169.
(18) Wang, J.; Zhang, P. C.; Lu, H. F.; Ma, N.; Wang, S.; Mao, H. Q.; Leong, K. W. *J. Controlled Release* **2002**, *83*, 157−165.
(19) Huang, S. W.; Wang, J.; Zhang, P. C.; Mao, H. Q.; Zhuo, R. X.; Leong, K. W. *Biomacromolecules* **2004**, *5*, 306−311.
(20) Wang, D. A.; Williams, C. G.; Yang, F.; Cher, N.; Lee, H.; Elisseeff, J. H. *Tissue Eng.* **2005**, *11*, 201−213.
(21) Libiszowski, J.; Kaluzynski, K.; Penczek, S. *J. Polym. Sci., Part A: Polym. Chem.* **1978**, *16*, 1275−1283.
(22) Pretula, J.; Kaluzynski, K.; Penczek, S. *Macromolecules* **1986**, *19*, 1797−1799.
(23) Richards, M.; Dahiyat, B. I.; Arm, D. M.; Lin, S.; Leong, K. W. *J. Polym. Sci., Part A: Polym. Chem.* **1991**, *29*, 1157−1165.